Received: 20 March 2020 | Revised: 14 May 2020 | Accepted: 21 May 2020

DOI: 10.1096/fj.202000668RR

RESEARCH ARTICLE

THE FASEB JOURNAL

Adaptation of rat fast-twitch muscle to endurance activity is underpinned by changes to protein degradation as well as protein synthesis

Stuart J. Hesketh[1] | **Hazel Sutherland**[1] | **Paulo J. Lisboa**[3] | **Jonathan C. Jarvis**[1] | **Jatin G. Burniston**[1,2]

[1]Research Institute for Sport & Exercise Sciences, Liverpool John Moores University, Liverpool, UK

[2]Liverpool Centre for Cardiovascular Science, Liverpool John Moores University, Liverpool, UK

[3]Department of Applied Mathematics,

Abstract

Muscle adaptations to exercise are underpinned by alterations to the abundance of individual proteins, which may occur through a change either to the synthesis or degradation of each protein. We used deuterium oxide (^2H_2O) labeling and chronic low-frequency stimulation (CLFS) in vivo to investigate the synthesis, abundance,

Abbreviations: 2DGE, two dimensional gel electrophoresis; ^2H, deuterium; ^2H_2O, deuterium oxide; AATC, aspartate aminotransferase, cytoplasmic; AATM, aspartate aminotransferase, mitochondrial; ABD, abundance; ABR, abundance rate; ACADL, long-chain specific acyl-CoA dehydrogenase, mitochondrial; ACON, aconitate hydratase, mitochondrial; ACTH, adrenocorticotropic hormone; ACTN1, alpha-actinin-1; ACTS/ACTC, actin, alpha skeletal muscle/ Actin, alpha cardiac muscle 1; ADH-1, alcohol dehydrogenase 1; ADR, absolute degradation rate; ALBU, serum albumin; ALDOA, fructose-bisphosphate aldolase A; ALDR, aldo-keto reductase family 1 member B1; ANXA4, annexin A4; ASR, absolute synthesis rate; AT2A2, sarcoplasmic/endoplasmic reticulum calcium ATPase 2; ATPA, ATP synthase subunit alpha, mitochondrial; ATPase, ATP synthase; ATPB, ATP synthase subunit beta, mitochondrial; ATPO, ATP synthase subunit O, mitochondrial; BSA, bovine serum albumin; Ca^{2+}, calcium ion; CAH3, carbonic anhydrase 3; CASQ1, calsequestrin-1; CHAPS, 3-[(3-Cholamidopropyl)dimethylammonio]-1-propanesulfonate hydrate; CLFS, Chronic low-frequency stimulation; CRYAB, alpha-crystallin B chain; Ctrl, non-stimulated contralateral control limb/muscle; CV, coefficient of variation; CX7A2, cytochrome c oxidase subunit 7A2, mitochondrial; DESM, desmin; DPP, dynamic proteome profiling; DTT, dithiothreitol; EDL, extensor digitorium longus; ENOB, beta-enolase; ESI-Q-TOF, electrospray ionisation quadrupole time of flight; FASP, filter aided sample preparation; FDL, flexor digitorium longus; FDR, false discovery rate; FHL1, four and a half LIM domains protein 1; FSR, fractional synthesis rate; G3P, glyceraldehyde-3-phosphate dehydrogenase; GC-MS, gas chromatography mass spectrometry; HBA, hemoglobin subunit alpha-1/2; HBB1, hemoglobin subunit beta-1; HBB2, hemoglobin subunit beta-2; HCl, hydrochloric acid; HSPB6, heat shock protein beta-6; IDH3A, isocitrate dehydrogenase [NAD] subunit alpha, mitochondrial; IDHP, isocitrate dehydrogenase [NADP], mitochondrial; IPG, immobilised pH gradient; k, synthesis rate constant; KAD1, adenylate kinase isoenzyme 1; KCRB, creatine kinase B-type; KCRM, creatine kinase M-type; KCRS, creatine kinase S-type, mitochondrial; KPYM, pyruvate kinase PKM; LC-MS, liquid chromatography mass spectrometry; LC-MS/MS, liquid chromatography mass spectrometry/mass spectrometry; LDHA, L-lactate dehydrogenase A chain; m_0, monoisotopic peak; m_1, m_2, m_3, heavy isotopomers; MALDI-TOF, Matrix-assisted laser desorption/ionization-time of flight; MALDI-TOF/MS, matrix-assisted laser desorption/ionization-time of flight/mass spectrometry; MDHC, malate dehydrogenase, cytoplasmic; MDHM, malate dehydrogenase, mitochondrial; MLRS, myosin regulatory light chain 2, skeletal muscle isoform; MLRV, myosin regulatory light chain 2, ventricular/cardiac muscle isoform; M_r, relative molecular mass; MS, mass spectrometry; MS/MS, tandem mass spectrometry; MyHC, myosin heavy chain; MYG, myoglobin; MYL1, myosin light chain 1/3, skeletal muscle isoform; MYL3, myosin light chain 3; n, number of exchangeable deuterium/hydrogen sites; NC, no change; NS, not significant; ODPA, pyruvate dehydrogenase E1 component subunit alpha, somatic form, mitochondrial; p, precursor enrichment; PARK7, protein/nucleic acid deglycase DJ-1; PFKAM, ATP-dependent 6-phosphofructokinase, muscle type; PGAM2, phosphoglycerate mutase 2; PGK1, phosphoglycerate kinase 1; PGM1, phosphoglucomutase-1; Phospho S/T, phosphorylation of serine/threonine; p*I*, isoelectric point; PLEC, plectin; Proteo-ADPT, absolute dynamic profiling technique for proteomics; PRVA, parvalbumin alpha; PYGB, glycogen phosphorylase, brain form; PYGM, glycogen phosphorylase, muscle form; SAFB1, scaffold attachment factor B1; SERCA, sarcoplasmic/endoplasmic reticulum calcium ATPase; SD, standard deviation; SDS, sodium dodecyl sulfate; Stim, stimulated limb/muscle; TA, tibialis anterior; TFA, trifluoroacetic acid; TIC, total ion chromatogram; TNNI1, troponin I, slow skeletal muscle; TNNI2, troponin I, fast skeletal muscle; TNNT1, troponin T, slow skeletal muscle; TNNT3, troponin T, fast skeletal muscle; TPIS, triosephosphate isomerase; TPM2, tropomyosin beta chain; TPM4, tropomyosin alpha-4 chain; UPLC, ultra performance liquid chromatography; VDAC, voltage-dependent anion channel.

Liverpool John Moores University, Liverpool, UK

Correspondence
Jatin G. Burniston, Research Institute for Sport & Exercise Sciences (RISES), Liverpool Centre for Cardiovascular Science (LCCS), Liverpool John Moores University, Tom Reilly Building, Byrom Street, Liverpool, L3 3AF, UK.
Email: j.burniston@ljmu.ac.uk

and degradation of individual proteins during exercise-induced muscle adaptation. Independent groups of rats received CLFS (10 Hz, 24 h/d) and ^2H_2O for 0, 10, 20, or 30 days. The extensor digitorum longus (EDL) was isolated from stimulated (Stim) and contralateral non-stimulated (Ctrl) legs. Proteomic analysis encompassed 38 myofibrillar and 46 soluble proteins and the rates of change in abundance, synthesis, and degradation were reported in absolute (ng/d) units. Overall, synthesis and degradation made equal contributions to the adaptation of the proteome, including instances where a decrease in protein-specific degradation primarily accounted for the increase in abundance of the protein.

KEYWORDS
biosynthetic labeling, chronic stimulation, deuterium oxide, protein degradation, protein synthesis

1 | INTRODUCTION

The adaptation of muscle to contractile activity underpins many of the health benefits of exercise and is a longstanding focus of interest in physiology. For example, endurance training profoundly alters substrate utilization and insulin sensitivity in muscle, and, thereby, has a positive impact on whole-body metabolism, disease risk, and aging. Proteins are the principal cellular components that determine the functional attributes of individual muscle fibres, including speed of contraction, fatigue resistance, and metabolism. Skeletal muscle adapts to exercise through quantitative changes in size and protein composition. Changes to the abundance of muscle proteins induced by exercise are long-established[1] and we have used non-targeted proteomics to investigate broad changes in muscle protein abundance of rats[2] and humans[3] in response to exercise training. Such profiling of protein abundance or posttranslational modifications captures detailed information on specific cell states. For example, protein abundance data has been incorporated into metabolic models[4] to reveal novel insights regarding energy metabolism during high-intensity exercise. Nevertheless, profiling of protein abundance data or protein posttranslational states do not capture dynamic aspects of the proteome, such as protein turnover, and cannot explain *how* changes in protein abundance are brought about in exercise-trained muscle.

Changes to protein abundance can only occur because proteins are dynamic and exist in a continuous cycle of synthesis and degradation, termed protein turnover. Protein turnover has long been studied using stable isotope-labeled amino acids in vivo and measurements of isotope enrichment in tissue amino acids[5] by gas-chromatography mass spectrometry (GC-MS). Exercise is a potent stimulus of protein synthesis in skeletal muscle and resistance and endurance exercise may regulate the synthesis of different populations of muscle proteins.[6] In humans, the fractional synthetic rate of mixed myofibrillar proteins is doubled 3 hours after an acute bout of resistance exercise[7] and the average turnover of proteins in endurance-trained muscle is 20% greater than in sedentary controls.[8] However, such data on average responses in mixed protein samples cannot distinguish whether, for example, the synthesis of all proteins increased by 50% or the synthesis of 50% of proteins was doubled. Recently, peptide mass spectrometry techniques have been combined with deuterium oxide labeling in vivo to generate data on the fractional synthesis rate (FSR) of individual proteins.[9] We developed this method further by incorporating protein abundance measurements,[5] which enabled increases in protein turnover to be distinguished from net increases in synthesis that lead to an accretion of new protein. Moreover, the measurement of protein abundance alongside protein-specific synthesis rates affords new opportunities to study protein dynamics in systems that are undergoing change.[10]

When measured at the level of individual proteins, changes in protein abundance that are not matched by equivalent changes to the synthetic rate of the protein may be attributed to protein degradation. In human muscle, we[10] reported protein-specific responses to resistance exercise, including proteins that changed in turnover rate without changing in abundance, and proteins that increased in abundance due to changes in the balance between degradation and synthesis. Our findings included proteins such as filamin C, whose increase in abundance after resistance exercise training without a measurable change in synthesis rate may, therefore, be attributed to a decrease in degradation rate. During the short 9-day investigation of resistance exercise training,[10] the majority of proteins that were responsive to exercise responded by increasing their turnover rate. For example, type IIa myosin heavy chain (MyHC) turnover was selectively increased during the first few sessions of resistance exercise, which may be a pre-sequel to the expected increase in type IIa MyHC abundance after sustained (eg, 16-week[11]) periods of training. Longer duration training studies are more likely to be associated with concomitant changes in muscle mass, which could

confound the interpretation of dynamic proteome profiling data reported in relative protein abundances and fractional rates of protein synthesis. Without the ability to provide information in absolute units it may not be possible to gain an entirely accurate understanding of the contributions that synthesis and degradation make to changes in the abundance of individual proteins.

In this paper, in contrast, we used an Absolute Dynamic Profiling Technique (ADPT) for proteomics, nicknamed "Proteo-ADPT" to measure protein abundances (ng) within the entire extensor digitorum longus (EDL) and report absolute rates (ng/d) of synthesis and degradation on a protein-by-protein basis. Adaptations to rat EDL were investigated during a 30-d period of unilateral chronic low-frequency stimulation (CLFS) in vivo. CLFS of rat fast-twitch muscle is a model of muscle transformation that has been widely used to investigate muscle plasticity.[12] CLFS provides uniform recruitment of muscle motor units and results in well-established time-dependent changes in the molecular, structural and functional properties of muscle.[13] The response of fast-twitch muscle to CLFS is similar to, but extends beyond the outcomes achieved by exercise models such as intensity-controlled treadmill running.[2] Unilateral stimulation of rat hindlimb dorsiflexor muscles in vivo provides stimulated and contralateral control muscles from each individual animal. In the current work, muscles were collected from independent groups of rats (n = 3, in each group) at 10-day intervals to enable high-quality data on isotope incorporation into proteins to be fitted to a single exponential model.[5] In rats, deuterium enrichment of the body water compartment occurs rapidly (within 30 minutes) after a bolus injection and can be maintained at a steady state by supplementation of the animals' drinking water, which simplifies protein synthesis calculations compared to studies in humans.[14] "Top-down" and "bottom-up" proteomic approaches were used to exploit the strengths of each technique. The myofibrillar proteome consists of numerous slow- and fast- isoforms which exhibit complex patterns of splice variation and posttranslational modification that are responsive to exercise training.[2,3] Therefore, myofibrillar proteoforms were resolved by 2-dimensional gel electrophoresis (2DGE) and spot densities were converted to absolute values.[15] Metabolic enzymes exhibit less complex proteoform responses to exercise and are more amenable to analysis at the peptide level, which offers broader inclusion of proteins at the extremes of MW and pI ranges. Therefore, abundances of soluble proteins were measured by spiking tryptic digests with yeast peptides prior to liquid chromatography tandem mass spectrometry (LC-MS/MS), which facilitates reporting of absolute protein data.[16] Proteo-ADPT enabled us to measure protein abundances (ng) of the entire EDL muscle and report absolute rates (ng/d) of synthesis and degradation on a protein-by-protein basis. Herein, we provide new insight to the processes underlying muscle adaptation. Our findings indicate protein degradation and synthesis make approximately equal contributions to the overall change in muscle phenotype. At the level of individual proteins, the response to the chronic endurance stimulus included instances where degradation rate was the primary factor underpinning an increase in protein abundance. Conversely, some individual decreases in protein abundance occurred primarily via a decrease in synthesis rate.

2 | MATERIALS AND METHODS

2.1 | Animals and experimental design

Experimental procedures were conducted under the British Home Office Animals (Scientific Procedures) Act 1986. Male Wistar rats (500 ± 69 g body weight; n = 12) were bred in-house in a conventional colony, housed in controlled conditions of 20°C, 45% relative humidity, and a 12 hours light (0600-1800 hours) and 12 hours dark cycle, with water and food available ad libitum.

Animals were assigned to four groups (n = 3 in each), including a sham-operated control group and three groups that received chronic low-frequency stimulation (CLFS; 10 Hz) of the left hindlimb dorsiflexor muscles, as described previously by our group.[13] Surgery was performed with aseptic precautions and the animals were anesthetized using a gaseous mixture of isoflurane and O_2. Buprenorphine (Temgesic, Indivior, Slough, UK) at a dose of 0.05 mg/kg^{-1} body mass, was administered pre-surgery for analgesia. Implantable stimulators were used according to Salmons and Jarvis[17] with minor modifications. Fine multi-stranded stainless-steel leads (Cooner Wire Assoc., Chatsworth, CA) were taken subcutaneously from the stimulator in the flank to just proximal to the knee on the left hind limb, the electrodes were fixed in close relationship to, but not in physical contact with, the common peroneal nerve. The body of the stimulator was situated in the abdominal cavity and held in place by suturing an integral Dacron mesh tag into the closure of the abdominal wall. The postoperative recovery of the animals was monitored daily for 1 week prior to commencing the stimulation protocol. The 0-day experimental time-point represents the sham-operated control group that were implanted with inactive stimulators and then, euthanized 1 week later. The remaining (10, 20, and 30 days) experimental groups had the stimulator activated non-invasively via an optical signal through the skin to a phototransistor in the device. Stimulation was initiated from day 0 at a continuous 10 Hz of the fast dorsiflexor muscles of the anterior compartment of the hind limb, including the EDL. Simultaneously, deuterium oxide (^2H_2O; Sigma-Aldrich, St. Louis, MO) administration was initiated by an intraperitoneal loading injection of 10 μL/g 99% ^2H_2O-saline, and then, maintained by administration of

5% (*v/v*) ^2H_2O in the drinking water available to the rats, as described previously.[18]

After 10, 20, and 30 days of CLFS and ^2H_2O consumption, animals were euthanized in a rising concentration of CO_2 followed by cervical dislocation. EDL muscles from the left stimulated limb (Stim) and the right non-stimulated limb (Ctrl) were isolated. Each muscle was cleaned of fat and connective tissue then weighed before being frozen in liquid nitrogen and stored at −80°C pending further analysis.

2.2 | Muscle processing

Muscles were fractionated into myofibrillar and soluble fractions according to Camera et al,.[10] Briefly, samples were pulverized under liquid nitrogen using a mortar and pestle. One-hundred milligrams of the tissue powder was homogenized on ice in 10 volumes of 1% Triton X-100, 50 mM Tris pH 7.4 including phosphatase inhibitor and complete protease inhibitor cocktails (Roche, Indianapolis, USA) using a PolyTron homogenizer. Samples were incubated on ice for 15 minutes, then centrifuged at 1000 *g*, 4°C, for 5 minutes. Supernatants containing soluble proteins were decanted and stored on ice, and the myofibrillar pellet was resuspended in 0.5 mL of homogenization buffer, then centrifuged at 1000 *g*, 4°C for 5 minutes. The washed myofibrillar pellet was solubilized in 10 volumes of 7 M urea, 2 M thiourea, 4% CHAPS, 30mM Tris, pH 8.5, and cleared by centrifugation at 12 000 *g*, 4°C, 45 minutes. Protein concentrations of each myofibrillar and soluble protein sample were measured using the Bradford assay (Sigma-Aldrich, Poole, Dorset, UK).

2.3 | Top-down proteomic analysis of myofibrillar proteins using 2DGE and MALDI mass spectrometry

Homogenates of the myofibrillar fraction were prepared for 2DGE as described previously.[2] Gels were produced in batches of eight, comprising individual gels for each left and right EDL from one animal in each group (0, 10, 20, and 30 days). An aliquot of each supernatant was precipitated in 5 volumes of acetone at −20°C for 1 hour then resuspended in 7 M urea, 2 M Thiourea, 2% (*w/v*) CHAPS, 20 mM dithiothreitol, 0.5% (*v/v*), and ampholytes (pH 3-11). Samples, containing 250 µg protein, were loaded on to 13 cm pH 3-11 nonlinear IPG strips (GE Healthcare, Chalfont St Giles, UK) and resolved using an "active rehydration" and isoelectric focusing protocol comprising: 150 Vh at 30 V, 300 Vh at 60 V, 500 Vh at 500 V, 1000 Vh at 1000 V, and 48 000 Vh at 8000 V; conducted on an IPGPhor II (GE Healthcare) at 20°C, maximum 50 mA per strip. IPG strips were equilibrated in 50 mM Tris-HCl pH 8.8, containing 6 M urea, 30% (*v/v*) glycerol, 70 mM SDS, and a trace of bromophenol blue. DTT (65 mM) was present as a reducing agent in the first equilibration and iodoacetamide (135 mM) in the second. Proteins were electrophoresed from the IPG strip through 16 cm linear 12% polyacrylamide gels at 20°C; at a constant current of 15 mA per gel for 30 minutes, then 30 mA per gel until the tracking dye reached the bottom edge of the gel. Gels were washed and stained with colloidal Coomassie blue (Bio-Safe; BioRad, Hercules, CA, USA) according to the manufacturer's instructions. Digitized images (8-bit gray scale, 300 dpi) of stained gels were saved as tagged-image file format (tiff) files.

2.4 | Myofibrillar protein abundance analysis

Image analysis (Samespots, v3.0, Nonlinear Dynamics, Newcastle, UK) was performed on the 24 individual 2DGE images, representing myofibrillar proteins from the EDL muscles of the stimulated and non-stimulated limb from n = 3 animals at each of the four experimental time points (0, 10, 20 and 30 days). Prominent spots were manually identified to avoiding including gel artifacts and the gel images were warped to align the spot positions to a common reference gel. The resulting spot outlines were applied to each parent image and manually verified, consistent with our previous work.[2]

2.5 | Identification of myofibrillar proteins using peptide mass fingerprinting

Gel spots were cut and processed using an Xcise robot (Proteome Systems, North Ryde, Australia) as described previously.[3] Gel plugs, destained in three changes of 25 mM ammonium bicarbonate in 50% acetonitrile were dehydrated before being incubated with 35 µL of 1.25 mg/mL porcine trypsin (Promega, Madison, WI, USA) in 50 mM ammonium bicarbonate. Peptide solutions were de-salted and concentrated (Zip-tips; Millipore, Billercia, MA, USA) before being mixed with matrix (3.5 µg α-cyano-4-hydroxcinnamic acid in 50:50 acetonitrile and 0.1% trifluoroacetic acid) and spotted on to 384-well stainless-steel target plates. A calibration mix (Laserbio Labs, Sophia Antipolis, France) consisting of angiotensin II (*m/z* 1046.2), angiotensin I (*m/z* 1296.5), neurotensin (*m/z* 1672.9), ACTH fragment {1-17} (*m/z* 2093.5), and ACTH fragment {18-39} (*m/z* 2465.19) was mixed 1:1 with matrix solution and spotted (0.5 µL) between every four sample-wells. Peptide mass spectra were recorded using a matrix-assisted laser desorption ionization tandem time of flight (MALDI-TOF/TOF) mass spectrometer (Axima TOF^2; Shimadzu Biotech, Manchester, UK) in positive reflectron mode over a mass/charge (*m/z*) range of 900-3000. Data were smoothed

(Gaussian, two channel peak width), baseline subtracted (100 channel peak width), and an adaptive (8.0^) threshold applied. Peptide mass lists (restricted to 20 peptides over 900-3000 m/z) were produced using the peak selection tool of the instrument's Launchpad software (Version 2.8.4) and searched against the UniProt database restricted to "Rattus" using a locally implemented MASCOT server (v.2.2.03; www.matrixscience.com). The enzyme specificity was set as trypsin allowing one missed cleavage, carbamidomethyl modification of cysteine (fixed), oxidation of methionine (variable), and an *m/z* error of ±0.3 Da.

Mass spectrometry data were recorded from every gel spot in every muscle sample (ie, left (stimulated) and right (non-stimulated) EDL from 0, 10, 20, and 30 days groups, n = 3 rats per group). Raw mass spectra were exported in mzXML format and mMass software (Version 5.5.0, http://www.mmass.org) was used to extract intensity data for the monoisotopic peak (m_0), m_1, and m_2 mass isotopomers of five selected peptides for each protein/ proteoform, as previously described.[18]

2.6 | Bottom-up analysis of soluble proteins using LC-MS/MS label-free quantitation

Soluble proteins in lysis buffer at a concentration of 5 μg/μL were processed for mass spectrometry by in-solution digestion according to the filter aided sample preparation (FASP) method.[19] Lysates containing 200 μg protein were precipitated in five volumes acetone at −20°C for 1 hour and the protein pellets were resuspended in 200 μL of UA buffer (8 M urea, 100 mM tris, pH 8.5). Samples were incubated at 37°C for 15 minutes in UA buffer with 100 mM dithiothreitol (DTT) followed by 20 minutes at 4°C in UA buffer containing 50 mM iodoacetamide (protected from light). Samples were washed twice with 100 μl UA buffer and transferred to 50 mM ammonium hydrogen bicarbonate (Ambic). Sequencing grade trypsin (Promega; Madison, WI, USA) in 50 mM Ambic was added at an enzyme to protein ratio of 1:50 and the samples were digested overnight at 37°C. To terminate digestion, peptides were collected in 50 mM Ambic and trifluoracetic acid (TFA) was added to a final concentration of 0.2% (v/v). Aliquots, containing 4 μg peptides, were desalted using C_{18} Zip-tips (Millipore, Billercia, MA, USA) and eluted in 50:50 of acetonitrile and 0.1% TFA. Peptide solutions were dried by vacuum centrifugation for 25 minutes at 60°C and peptides were resuspended in 0.1% formic acid (FA) spiked with 10 fmol/μL yeast ADH1 (Waters Corp.) in preparation for LC-MS/MS analysis.[16]

2.7 | Liquid chromatography-mass spectrometry

Label-free liquid chromatography-mass spectrometry analysis was performed using nanoscale reverse-phase ultra-performance liquid chromatography (UPLC; Nano Acquity; Waters) and online electrospray ionization quadrupole–time-of-flight mass spectrometry (ESI-Q-TOF; QTOF Premier; Waters). Samples (1 μg tryptic peptides) were loaded in aqueous 0.1% (v/v) FA via a Symmetry C_{18} 5 μm, 2 cm, 180 μm trap column (Waters). Separation was conducted at 35°C via a BEH C_{18} 1.7 μm, 25 cm, 75 μm analytical reverse-phase column (Waters). Peptides were eluted using a gradient that rose to 37.5% acetonitrile 0.1% (v/v) FA over 90 minutes at a flow rate of 300 nL/min. For all measurements, the mass spectrometer was operated in positive electrospray ionization mode at a resolution of >10,000 full width at half maximum. Before analysis, the time-of-flight analyzer was calibrated using fragment ions of [Glu-1]-fibrinopeptide B from *m/z* 50-1990. Mass spectra (MS) for liquid chromatography-mass spectrometry profiling were recorded between 350 and 1600 *m/z* using mass spectrometry survey scans of 0.45-seconds duration with an inter scan delay of 0.05 seconds. In addition, equivalent data-dependent tandem mass spectrometry (MS/MS) spectra were collected from each 0 days (control) sample. MS/MS spectra of collision-induced dissociation fragment ions were recorded for the five most abundant precursor ions of charge 2+ or 3+ detected in the survey scan. Precursor fragmentation was achieved by collision-induced dissociation at an elevated (20-40 eV) collision energy over a duration of 0.15 s per parent ion with an inter scan delay of 0.05 s over 50-2000 *m/z*. Acquisition was switched from MS to MS/MS when the base peak intensity exceeded a threshold of 30 counts/s, and returned to the MS mode when the total ion chromatogram (TIC) in the MS/MS channel exceeded 10 000 counts or when 1.0 s (5 scans) were acquired. To avoid repeated selection of peptides for MS/MS, the program used a 30-seconds dynamic exclusion window.

Progenesis QI for proteomics (Nonlinear Dynamics, Newcastle, UK) was used to perform label-free quantitation (LFQ) consistent with our previous work.[20-23] Prominent ion features (>600 per chromatogram) were used as vectors to align each data set to a reference chromatogram. An analysis window of 15-105 minutes and 350-1500 *m/z* was selected. Log-transformed MS data were normalized by inter-sample abundance ratio, and differences in relative protein abundance were investigated using nonconflicting peptides only.

MS/MS spectra were exported in Mascot generic format and searched against the Swiss-Prot database restricted to Rattus (8,071 sequences) using a locally implemented Mascot server (v.2.2.03; www.matrixscience.com). Enzyme specificity was trypsin, which allowed one missed cleavage, carbamidomethyl modification of cysteine (fixed), deamination of asparagine and glutamine (variable), oxidation of methionine (variable), and an m/z error of ± 0.3 Da. Mascot output (xml format), restricted to nonhomologous protein identifications, was recombined with MS profile data, and peptides modified by deamination or oxidation were removed before quantitative analysis.

Mass isotopomer abundance data were extracted from MS only spectra using Progenesis QI (Nonlinear Dynamics). Peak picking was performed on ion features with +2, or +3 charge states within an analysis window of 15-105 minutes and 350-1500 *m/z*. The abundance of the monoisotopic peak (m_0), m_1, m_2, and m_3 mass isotopomers were collected over the entire chromatographic peak for each nonconflicting peptide that was used for LFQ, as previously described.[10]

2.8 | Calculation of individual protein synthesis rates

The FSR of each protein was calculated in stimulated and contra-lateral non-stimulated (control) muscles.

Precursor enrichment was back calculated from peptide mass isotopomer data according to.[18] Briefly the enriched molar fraction of each mass isotopomer was calculated by subtracting the molar fraction of the unlabeled control peptide from the equivalent ^2H_2O-labeled peptide, and the enrichment ratio between m_2 and m_1 mass isotopomers was used to calculate precursor enrichment (p) using:

$$p = \left(\left(\frac{EM_2}{EM_1} \right) \Big/ \frac{(n-1)}{2} \right) \cdot 100 \quad (1)$$

Where EM_1 is the enriched molar fraction of m_1 and EM_2 is the enriched molar fraction of m_2 and n is the number of H-D exchange sites counted by referencing the peptide amino acid sequence against standard tables.[24] The median precursor enrichment of each animal was derived from peptides belonging to serum albumin (ALBU) and this value of p was used in 5 to calculate the FSR of individual peptides.

Protein FSR were calculated from the incorporation of deuterium into newly synthesized protein, which results in a decrease in the molar fraction (fm_0) of the monoisotopic (m_0) peak.

$$fm_0 = \frac{m_0}{m_0 + m_1 + m_2 + m_3} \quad (2)$$

The rate constant (k) for the decay of fm_0 was calculated using semi-log plots to fit a linear model ($y = k \cdot x + c$) to the change (Δ) in log-transformed fm_0 data across 0, 10, 20, and 30 days, as a function of time.

$$k = \frac{\Delta(-\ln(fm_0)) - c}{\Delta\,(\text{time})} \quad (3)$$

Data were filtered to exclude peptides with a goodness of fit, R-squared (R^2), to the linear model of <0.85. In addition, the rate constant (k) for the decay of fm_0 was also calculated as a first-order exponential spanning from the beginning (t) to end (t') of each 10-day labeling period, for example, 0-10, 10-20 days, etc, using Equation (4).

$$k = \frac{1}{t' - t} \cdot -\ln\left(\frac{fm_{0t}}{fm_{0t'}} \right) \quad (4)$$

Regardless of whether Equations (3) or (4) is used, the calculation of FSR from k depends on the number (n) of ^2H exchangeable H–C bonds, which was calculated by referencing each peptide sequence against standard tables.[24] Peptide FSR was derived by dividing k by the molar percent enrichment of deuterium in the precursor (p) pool and the total number (n) of ^2H exchangeable H–C bonds in each peptide.

$$\text{FSR} = \frac{k}{(n \cdot p)} \quad (5)$$

Protein FSR was reported as the median value of peptides unique to each protein. Decimal values were multiplied by 100 to give FSR in %/d.

2.9 | Calculation of absolute muscle protein data

Relative data (eg, density of 2DGE spots, LFQ of soluble peptides, and protein specific FSR) were converted to absolute values for each muscle. Total protein extracted from each muscle fraction was calculated.

$$\text{Protein content} = \left(\frac{\text{PC} \cdot \text{HV}}{\text{MP}} \right) \cdot \text{WW} \quad (6)$$

The yield of protein extracted per mg of muscle powder was calculated from the concentration of myofibrillar or soluble protein (PC; mg/mL) measured by protein assay, multiplied by the volume (mL) of homogenate (HV) and divided by the mass (mg) of aliquoted muscle powder (MP). The yield of soluble and myofibrillar proteins per mg of muscle powder was multiplied by muscle wet weight (WW) to calculate the protein content (mg).

The normalized relative abundance (ABD_{rel}) of proteins in the soluble fraction was calculated by LFQ against 50 fmol yeast alcohol dehydrogenase (ADH1_Yeast) that was spiked into each sample after tryptic digestion. Relative abundance ABD_{rel} data in fmol/ µg peptide digest were multiplied by total protein content (µg) of the soluble fraction to calculate absolute protein abundance (ABD_{abs}) in pmol.

$$ABD_{abs} = \frac{\text{Protein content} \cdot ABD_{rel}}{1000} \quad (7)$$

Mole abundance data (ABD_{abs}) were converted to absolute (μg) values using:

$$ABD = MW \cdot ABD_{abs} \quad (8)$$

Where MW is the protein molecular weight (kDa) specified in the UniProt database and ABD_{abs} is the mole abundance of the protein from Equation (7) expressed in fmol.

Absolute abundance (ABD) of proteins in the myofibrillar fraction was calculated by converting spot density (AU) into μg values.[25]

$$ABD = \left(\left(\frac{\text{Gel protein load}}{\text{Total spot density}} \right) \cdot \text{Spot density} \right) \cdot 4 \quad (9)$$

The protein load (250 μg) of each gel was divided by the sum density of all spots to give a conversion factor for each gel. Individual spot densities were multiplied by the gel conversion factor to give abundance values/μg protein loaded on each gel. Spot abundance data were multiplied by the total content of myofibrillar protein to derive the absolute abundance (μg) of each protein in each muscle.

The absolute synthesis rate (ASR) of individual proteins was calculated by multiplying protein abundance (pg) by the decimal FSR.

$$ASR = ABD \cdot FSR \quad (10)$$

The rate of change in protein abundance was calculated by converting the difference in abundance between stimulated and contra-lateral control muscle into abundance rate (ABR) change from the beginning (t) to end (t') of each labeling period.

$$ABR = \frac{1}{t' - t} \cdot \left(ABD_{t'} - ABD_{t} \right) \quad (11)$$

Absolute degradation rate (ADR) was calculated as the difference between ASR and the rate of change in abundance.

$$ADR = ASR - ABR \quad (12)$$

2.10 | Statistical analysis

Unless stated otherwise, data are presented as mean ± standard deviation (SD) and statistical analyses were conducted in *R* (version 3.6.2). One factor analysis of variance (ANOVA) was used to test the consistency of data in control non-stimulated muscle over the duration (0–30 days) of the experimental period. At each time point, differences between stimulated and contra-lateral control were investigated using Student's paired *t* tests. Significance data were controlled for multiple testing using the Benjamini-Hochberg (BH) procedure.

3 | RESULTS

Surgical implantation of stimulators in preparation for unilateral CLFS in vivo did not significantly affect either the wet weight (Figure 1A) or protein abundance profile (Figure 1B) of EDL muscle (Day 0 time point). There was also no significant change in the wet weight or protein profile (Figure 1A and 1C, respectively), of the non-stimulated control (Ctrl) EDL at the end of the experimental period. In response to CLFS, the wet weight (92 ± 8 mg) of stimulated (Stim) EDL was 50% less ($P < .05$) than the contralateral Ctrl (185 ± 16 mg) after the 30-day intervention (Figure 1A).

"Top-down" analysis of myofibrillar proteins was performed to investigate the multiple proteoforms of myofibrillar proteins. 2DGE is optimized for this purpose and resolved 43 protein spots in each Stim and Ctrl EDL (total of 24 samples, n = 3 biological replicates at 0, 10, 20, and 30 days experimental time points). MS were recorded only from in-gel digests of each spot present in every biological sample (approximately 1000 gel spots analyzed). After filtering based on quality control criteria, a total of 30 spots had complete data from five peptides per protein present in all samples. In addition, a further eight spots were detected by the same criterion only in Stim samples after > 20 days CLFS. The total number of nonredundant protein identifications from top-down analysis was 23, and 10 proteins were resolved to multiple proteoforms. Supporting Information illustrates the gel position of the 38 spots that satisfied the requirements for protein synthesis calculations and provides the identity of each gel spot. "Bottom-up" analysis of soluble proteins by LC-MS/MS yielded a list of 46 proteins that had at least one protein-specific peptide with a good fit ($R^2 > 0.85$) to the nonlinear model and were detected in all (n = 24) Ctrl and Stim samples. The majority of soluble proteins identified were enzymes of either mitochondrial/oxidative metabolism or glycolysis/anaerobic metabolism.

At the onset of the experiment there were no significant differences in protein abundance between sham-operated and Ctrl muscle, the Pearson correlation coefficient (r) for protein abundance was $r = .9899$ (Figure 1B) and the median coefficient of variation was 20.2%. Protein abundance profiles were consistent in Ctrl EDL throughout the experiment. The Pearson correlation coefficient for protein abundance between Ctrl muscle at day 0 and day 30 of the experiment was $r = .9997$ (Figure 1C), the median and interquartile range in coefficient of variation was 2.45% (IQR: 0.5%-2.66%) demonstrating high levels of reproducibility for our analysis in Ctrl unstimulated EDL.

Statistically significant ($P < .05$ BH-corrected) differences in protein abundance were detected in Stim EDL and became more numerous from 20 to 30-days time points (Figure 1D-F). The changes in myofibrillar protein

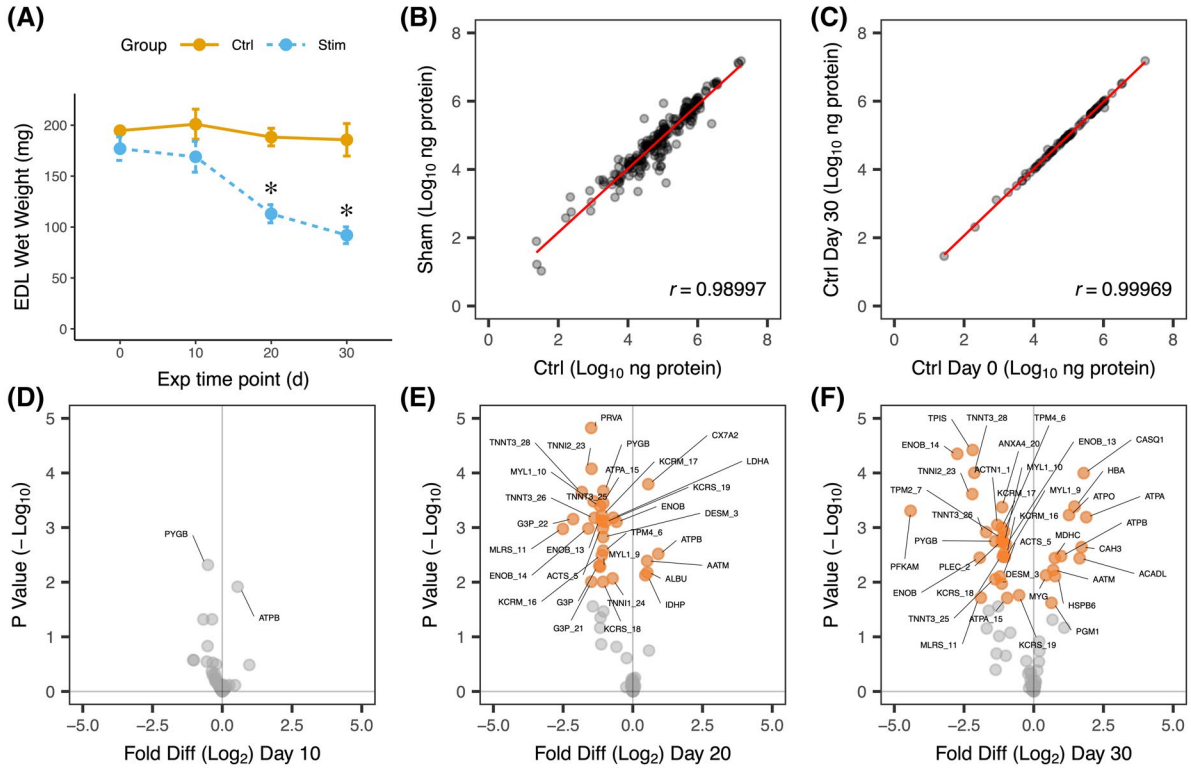

FIGURE 1 Temporal adaptation of EDL to chronic low-frequency stimulation in vivo. A, Wet weight (mg) of extensor digitorum longus (EDL) stimulated (Stim) at 10 Hz and contralateral non-stimulated control (Ctrl). Data are presented as mean ± SD from independent groups of n = 3 rats at each time point *$P < .05$ statistically significant difference between Stim and Ctrl assessed using paired t-tests at each experimental time point. B, Pearson correlation coefficient (r) in total abundance (ng) of n = 76 proteins quantified in EDL of n = 3 sham-operated and contralateral Ctrl limbs representing the beginning (day 0) of the experimental period. C, Correlation (r) in protein abundances (n = 76) quantified in Ctrl EDL at the beginning (day 0) and end (day 30) of the experimental period (n = 3, biological replicates). Fold differences (Diff) in protein abundance between Stim and Ctrl EDL after 10 days (D), 20 days (E), or 30 days (F) of unilateral chronic low-frequency stimulation (CLFS). Proteins that changed significantly ($P < .05$, BH-corrected) in Stim muscle are colored and labeled by their UniProt identifier

abundance were consistent with a shift toward a slower phenotype in Stim EDL. The fast isoform of troponin T (TNNT3) was resolved as three separate proteoforms (spots 25, 26, 28), each of which decreased after 30 days CLFS. The slow isoforms of myosin regulatory (MLRV) and essential (MYL3) light chains were absent in Ctrl EDL and first emerged after 10 and 20 days CLFS, respectively. In addition, new proteoforms of TNNT1 (spots 33, 34) were detected after 20 days CLFS. Table 1 provides a summary of new proteoforms that emerged in Stim EDL.

Changes in the soluble fraction agreed with the shift in myofibrillar proteoforms indicative of a more oxidative, slow-twitch phenotype. After 10 days CLFS, the total abundance of ATP synthase-alpha (ATPA) increased (1.46-fold, $P = .0121$, FDR = 46%) and the so-called brain isoform of glycogen phosphorylase (PYGB) decreased (1.43-fold, $P = .0048$, FDR = 37%). After 20 days CLFS (Figure 1E), there were further increases in the abundance of enzymes involved in aerobic metabolism. The abundance of ATP synthase-beta (ATPB) became 1.88-fold greater ($P = .011$ BH-corrected) in Stim (82.36 µg) compared to Ctrl (43.66 µg) and cytochrome C oxidase subunit 7A2 (CX7A2) abundance increased from 6.05 µg to 8.9 µg ($P = .0034$ BH-corrected). These changes cooccurred alongside significant decreases in the abundance of the calcium handling protein, parvalbumin (PRVA), and enzymes involved in glycolytic metabolism, including beta-enolase, (ENOB), glyceraldehyde-3-phosphate dehydrogenase (G3P), and the muscle isoform of lactate dehydrogenase (LDHA). EDL muscle exposed to 30 days CLFS (Figure 1F) exhibited further decreases in the abundance of glycolytic enzymes, including triosephosphate isomerase (TPIS) and phosphofructokinase (PFKAM), which were 4.68-fold and 2.14-fold less ($P < .05$ BH-corrected) abundant in Stim EDL. Whereas alpha- and beta- subunits of ATP synthase were 3.69- and 1.98-fold more ($P < .05$ BH-corrected) abundant in Stim EDL (Figure 1F).

The FSR among all 76 proteins measured across 0 to 30 days time points (Equation 3) in n = 3 biological replicates averaged 4.97 ± 3.9%/d in Ctrl and 5.18 ± 4.18%/d in Stim muscle. Protein-specific FSR ranged from 0.55 ± 0.15%/d (Plectin, PLEC_2) to 17.02 ± 5.01%/d (carbonic anhydrase

TABLE 1 Emergent proteins in CLFS muscle

Identifier	20 days ABD (µg) 30 days ABD (µg)	20-30 days FSR (%/d)	20-30 days ABR (ng/d)	20-30 days ASR (ng/d)	20-30 days ADR (ng/d)
CRYAB_35*	18.88 ± 1.89 19.73 ± 5.23	2.47 ± 0.43	85.51 ± 372.03	480 ± 138	394 ± 238
KCRS_32*	37.96 ± 5.23 39.71 ± 19.47	4.9 ± 0.57	174.22 ± 3,243.97	1,898 ± 145	1724 ± 3,219
MLRV_31*	44.24 ± 9.43 44.60 ± 5.20	1.59 ± 0.56	36.88 ± 782.42	712.15 ± 307.97	675.27 ± 738.01
MYL3_36	47.03 ± 15.05 54.83 ± 23.03	3.87 ± 0.85	780.11 ± 1,022.84	1,938.64 ± 660,61	1,158.54 ± 1,102.79
MYL3_37	29.68 ± 3.32 35.47 ± 7.05	4.21 ± 0.33	578.82 ± 624.54	1,369.02 ± 213.76	790.21 ± 622.45
MYL3_38	70.88 ± 11.13 84.77 ± 11.03	2.13 ± 0.28	1,388.91 ± 2,097.22	1,662.47 ± 283.74	273.56 ± 2,204.61
TNNT1_33*	30.72 ± 14.42 60.21 ± 10.84	2.66 ± 0.23	2,948.85 ± 2,439.33	1,211.08 ± 184.20	-1737.78 ± 2,595.90
TNNT1_34*	22.16 ± 1.30 24.03 ± 3.36	3.61 ± 0.34	187.26 ± 299.58	831.54 ± 59.44	644.28 ± 253.55

Note: Data are presented for proteins that emerged in EDL after >20 days CLFS. Identifier represents the UniProt identifier and 2DGE spot number of each proteoform, *represents proteoforms that may also have been detected in some replicates after 10 days CLFS. Total abundance (ABD) of each proteoform after 20 or 30 days CLFS is presented (µg). Fractional synthesis rate (FSR, %/d) was calculated between 20 days and 30 CLFS using Equation (4). The absolute rate of abundance change (ABR), synthesis (ASR) and degradation (ADR) are presented in ng/d.

3, CAH3_29). The distribution of synthesis data were strikingly different when reported in absolute (ng/d) units and linear regression found that FSR explained <15% of the difference ASR (Figure 2A). The ASR of proteins in Ctrl muscle spanned three orders of magnitude from 0.34 ± 0.19 ng/d (four-and-a-half LIM domains protein 1; FHL1) to 292.78 ± 20.07 µg/d (tropomyosin alpha-4; TPM4). In keeping with the unchanging abundance of proteins in Ctrl muscle (Figure 1C), the ASR of proteins in non-stimulated EDL did not differ over the 30-d experimental period. The ADR of each protein was calculated from differences between the rate of change in protein abundance (absolute abundance rate; ABR) and the absolute rate of protein synthesis during the experimental period. Accordingly, there was no difference in protein ADR in Ctrl muscle during the 30-d experimental period. Proteo-ADPT data for each protein studied is presented in Table 2.

Figure 2 summarises the numbers of proteins that exhibited significant ($P < .05$ BH-corrected) differences over the entire 30-d CLFS intervention. Volcano plots of the fold-change and significance of individual protein FSR, ASR, and ADR are provided in Figure 2C-E, respectively. After 30 days CLFS there were 34 significant ($P < .05$ BH-corrected) differences in protein-specific FSR (Figure 2C). The FSR of glycolytic enzymes such as TPIS was less in Stim (0.9 ± 0.02%/d) than Ctrl (2.05 ± 0.04%/d), whereas mitochondrial proteins were common among the proteins that had significantly greater FSR in Stim EDL. A similar pattern was evident when the absolute synthesis rate (ASR; ng/d) of individual proteins was compared (Figure 2D). There were 23 significant ($P < .05$ BH-corrected) differences in protein-specific ASR. The ASR of TPIS in Stim (375.5 ± 18.2 ng/d) was 3.2-fold less than Ctrl (1187.2 ± 42.2 ng/d), whereas the ASR of ATP synthase alpha (ATPA) was 6294 ± 958.6 ng/d in Stim and 1181 ± 226.9 ng/d in Ctrl. Twelve proteins exhibited greater ($P < .05$ BH-corrected) degradation in Stim than Ctrl muscle after 30 days CLFS (Figure 2E). For example, the ADR of plectin (PLEC_2) was 24 807 ± 856 ng/d in Stim and 5584 ± 1706 ng/d in Ctrl muscle.

Six proteins: carbonic anhydrase 3 (CAH3), calsequestrin (CASQ1), heat shock protein 20 (HSPB6), mitochondrial creatine kinase (KCRS_19), fast troponin T (TNNT3_25), and triosephosphate isomerase (TPIS) exhibited significant differences in FSR, ASR, and ADR (Figure 2B). CASQ1, HSPB6, and KCRS_19 exhibited greater FSR, ASR, and ADR in Stim muscle, indicating enhanced turnover of these proteins in addition to the significant gains in the abundance of these proteins reported in Figure 1F. In contrast, TPIS exhibited lesser FSR and ASR but greater ADR in Stim, indicating that changes in both synthesis and degradation contributed to the change in TPIS abundance.

Figure 2F shows the percent contribution that degradation made to the significant changes in protein abundance. Overall, degradation contributed 49% to the changes in

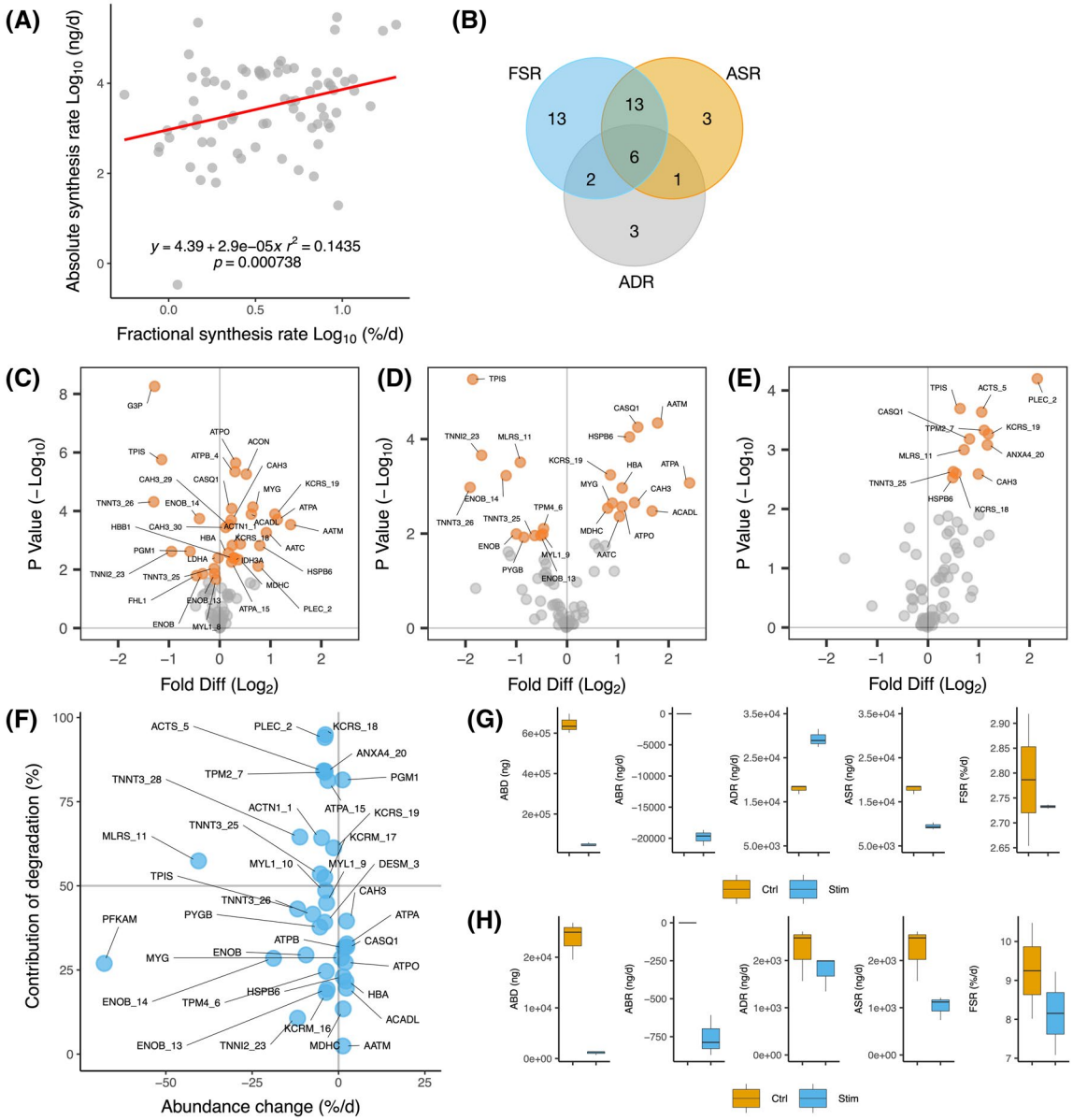

FIGURE 2 Dynamic responses of EDL muscle from 0-30 days of chronic -low-frequency stimulation. A, Distribution of individual protein fractional (FSR) and absolute (ASR) synthesis rates in Ctrl muscle calculated from data collected at 0, 10, 20, and 30 days experimental time points using Equation (3). B, Venn diagram illustrating the numbers of proteins that shared significant ($P < .05$ BH-corrected) differences in fractional synthesis rate (FSR), absolute synthesis rate (ASR) and absolute degradation rate (ADR). Volcano plots illustrating fold differences (Diff) in protein FSR (C), ASR (D), and ADR (E) in Stim compared to Ctrl EDL after 30-d CLFS. Proteins that differed significantly ($P < .05$, BH-corrected) in Stim muscle are colored and labeled by their UniProt identifier. F, Percent contribution of degradation to significant ($P < .05$ BH-corrected) changes in protein abundance. Protein abundance change (%) represents the rate (ng/d) of change in abundance expressed as a percentage of the average protein abundance during the 30-d experimental period. (G and H) Box plots reporting total protein abundance (ABD, ng), rate of change in abundance (ABR, ng/d), absolute synthesis rate (ASR, ng/d), absolute degradation rate (ADR, ng/d), and FSR (%/d) for (G) fast skeletal muscle myosin regulatory light chain (MLRS) proteoform 11 and (H) phosphofructokinase (PFKAM)

protein abundance calculated over the entire 30-day experimental period. There was a broad distribution in the relative contributions of synthesis and degradation to the significant changes in protein abundance. The abundance of phosphofructokinase (PFKAM) decreased at a rate of 754.95 ng/d from 23.76 ± 3.79 µg per muscle in Ctrl to 1.1 ± 0.38 µg per muscle in Stim during the course of the 30-day experiment (Figure 2G). The average difference in ASR between Stim (1023 ng/d) and Ctrl (2219 ng/d) was 1196 ng/d. Whereas the difference in ADR between Stim (1778 ng/d) and Ctrl (2219 ng/d) was 441 ng/d. Therefore, the 1196 ng/d lesser ASR combined with the 441 ng/d lesser in ADR in Stim accounts for the 755 ng/d change in PFKAM abundance. Proteo-ADPT data for each of the 76 proteins investigated are provided in Table 2.

TABLE 2 Proteo-ADPT data 0-30 days CLFS

Identifier	Group	ABD (µg)	FSR (%/d)	ASR (ng/d)	ABR (ng/d)	ADR (ng/d)
AATC	Ctrl	43.592 ± 3.384	0.88 ± 0.07	383.68 ± 3.32	0 ± 0	383.68 ± 3.32
	Stim	50.003 ± 4.554	1.67 ± 0.11	784.84 ± 119.29	213.68 ± 42.39	571.16 ± 81.89
AATM	Ctrl	34.221 ± 4.305	0.87 ± 0.04	298.96 ± 38.68	0 ± 0	298.96 ± 38.68
	Stim	55.58 ± 5.454	2.3 ± 0.21	1028.94 ± 54.35	711.95 ± 230.48	317 ± 281.59
ACADL	Ctrl	8.162 ± 3.68	2.61 ± 0.04	212.68 ± 95.31	0 ± 0	212.68 ± 95.31
	Stim	25.567 ± 3.297	4.02 ± 0.16	679.15 ± 87.14	580.15 ± 198.98	99.01 ± 205.11
ACON	Ctrl	78.282 ± 10.375	5.07 ± 0.04	3967.9 ± 554.63	0 ± 0	3967.9 ± 554.63
	Stim	89.169 ± 11.258	7.28 ± 0.11	6100.55 ± 830.82	362.9 ± 257.26	5737.66 ± 841.53
ACTA	Ctrl	61.161 ± 11.523	1.01 ± 0.01	617.14 ± 112.47	0 ± 0	617.14 ± 112.47
	Stim	58.469 ± 6.794	1.53 ± 0.27	901.62 ± 52.84	−89.74 ± 160.83	991.36 ± 139.02
ACTN1_1	Ctrl	405.496 ± 30.172	4.26 ± 0.17	17314.46 ± 1948.02	0 ± 0	17314.46 ± 1948.02
	Stim	164.731 ± 35.286	5.07 ± 0.07	14445.82 ± 1574.07	−8025.48 ± 870.36	22471.3 ± 1721.73
ACTS_5	Ctrl	15168.203 ± 1309.041	1.48 ± 0.18	222450.22 ± 11174.94	0 ± 0	222450.22 ± 11174.94
	Stim	6607.98 ± 2706.648	1.63 ± 0.2	177259.56 ± 34551.35	−285340.78 ± 47017.47	462600.34 ± 31187.12
ALBU	Ctrl	243.555 ± 13.654	7.1 ± 0.09	17292.04 ± 1143.14	0 ± 0	17292.04 ± 1143.14
	Stim	247.663 ± 17.125	7.26 ± 0.03	17831.57 ± 1002.56	136.95 ± 314.03	17694.62 ± 938.63
ALDOA	Ctrl	105.533 ± 8.929	8.57 ± 0.07	9041.99 ± 718.92	0 ± 0	9041.99 ± 718.92
	Stim	107.591 ± 13.154	8.43 ± 0.33	8966.08 ± 352.68	68.61 ± 504.91	8897.48 ± 486.85
ALDR	Ctrl	14.857 ± 5.685	8.31 ± 0.48	1252.86 ± 547.75	0 ± 0	1252.86 ± 547.75
	Stim	14.576 ± 2.829	8.35 ± 0.19	1233.66 ± 372.77	−9.35 ± 121.2	1243.01 ± 477.47
ANXA4_20	Ctrl	96.002 ± 6.515	1.21 ± 0.09	1167.16 ± 167.96	0 ± 0	1167.16 ± 167.96
	Stim	44.042 ± 4.98	1.27 ± 0.08	891.6 ± 124.51	−1731.99 ± 128.43	2623.59 ± 223.16
AT2A2	Ctrl	291.584 ± 27.49	1.39 ± 0.35	4022.31 ± 820.52	0 ± 0	4022.31 ± 820.52
	Stim	273.248 ± 28.487	1.52 ± 0.34	4233.8 ± 632.36	−611.17 ± 1132.4	4844.98 ± 1549.32
ATPA	Ctrl	84.809 ± 29.446	1.44 ± 0.23	1181.01 ± 226.93	0 ± 0	1181.01 ± 226.93
	Stim	312.892 ± 28.477	3.16 ± 0.03	6293.98 ± 958.65	7602.77 ± 332.85	−1308.79 ± 1042.17
ATPA_15	Ctrl	208.838 ± 34.349	2.66 ± 0.14	5580.88 ± 1207.51	0 ± 0	5580.88 ± 1207.51
	Stim	108.746 ± 30.784	3.13 ± 0.05	4957.02 ± 922.48	−3336.41 ± 383.08	8293.43 ± 1108.25
ATPB	Ctrl	79.212 ± 17.137	8.93 ± 0.49	7051.56 ± 1408.75	0 ± 0	7051.56 ± 1408.75
	Stim	156.501 ± 12.825	10.04 ± 0.72	11845.89 ± 1622.98	2576.27 ± 603.41	9269.62 ± 1567.04
ATPB_4	Ctrl	1706.319 ± 145.531	9.07 ± 0.03	154731.89 ± 12664.85	0 ± 0	154731.89 ± 12664.85
	Stim	1739.905 ± 2094.648	11.18 ± 0.1	193243.78 ± 116927.47	1119.53 ± 71444.82	192124.25 ± 47124.97
ATPO	Ctrl	15.344 ± 3.419	6.7 ± 0.06	1027.14 ± 223.81	0 ± 0	1027.14 ± 223.81
	Stim	36.871 ± 1.609	8.32 ± 0.03	2173.76 ± 199.42	717.59 ± 88.62	1456.18 ± 270.06
CAH3	Ctrl	21.315 ± 1.457	14.55 ± 0.28	3101.48 ± 228.51	0 ± 0	3101.48 ± 228.51
	Stim	70.147 ± 12.132	17.02 ± 0.17	7792.69 ± 1141.01	1627.74 ± 398.03	6164.95 ± 757.58
CAH3_29	Ctrl	852.223 ± 77.549	17.15 ± 0.14	146241.07 ± 14426.05	0 ± 0	146241.07 ± 14426.05
	Stim	759.728 ± 874.42	19.5 ± 0.32	157847.21 ± 83637.41	−3083.16 ± 30795.48	160930.38 ± 53221.33
CAH3_30	Ctrl	980.578 ± 82.811	20.43 ± 0.26	200225.26 ± 14453.65	0 ± 0	200225.26 ± 14453.65
	Stim	998.806 ± 1254.078	22.15 ± 0.06	219412.19 ± 133930.1	607.62 ± 43600.38	218804.57 ± 90655.57
CASQ1	Ctrl	0.205 ± 0.023	9.47 ± 0.18	19.43 ± 2.36	0 ± 0	19.43 ± 2.36
	Stim	0.71 ± 0.052	11.16 ± 0.01	51.05 ± 1.92	16.83 ± 2.41	34.22 ± 1.26
CX7A2	Ctrl	6.084 ± 0.287	7.27 ± 0.04	442.56 ± 21.29	0 ± 0	442.56 ± 21.29
	Stim	6.367 ± 0.946	7.33 ± 0.36	457.11 ± 53.43	9.42 ± 36.85	447.69 ± 32.45

(Continues)

TABLE 2 (Continued)

Identifier	Group	ABD (µg)	FSR (%/d)	ASR (ng/d)	ABR (ng/d)	ADR (ng/d)
DESM_3	Ctrl	709.712 ± 59.405	4.44 ± 0.27	31389.53 ± 928.18	0 ± 0	31389.53 ± 928.18
	Stim	322.224 ± 134.632	4.55 ± 0.24	23533.83 ± 4603.63	−12916.29 ± 3088.12	36450.12 ± 1941.28
ENOB	Ctrl	12.279 ± 2.435	8.5 ± 0.46	1040.21 ± 188.98	0 ± 0	1040.21 ± 188.98
	Stim	3.208 ± 0.794	6.75 ± 0.56	520.96 ± 53.5	−302.38 ± 107.36	823.34 ± 147.25
ENOB_13	Ctrl	126.88 ± 9.134	7.2 ± 0.19	9146.97 ± 894.84	0 ± 0	9146.97 ± 894.84
	Stim	63.812 ± 11.828	6.7 ± 0.09	6385.87 ± 581.45	−2102.28 ± 277.56	8488.14 ± 527.53
ENOB_14	Ctrl	122.248 ± 8.739	8.32 ± 0.2	10182.92 ± 974.33	0 ± 0	10182.92 ± 974.33
	Stim	18.397 ± 3.475	6.31 ± 0.16	4431.45 ± 265.25	−3461.71 ± 194.53	7893.16 ± 445.04
FHL1	Ctrl	0.029 ± 0.014	1.12 ± 0.13	0.34 ± 0.2	0 ± 0	0.34 ± 0.2
	Stim	0.029 ± 0.022	0.82 ± 0.02	0.24 ± 0.15	−0.01 ± 0.34	0.24 ± 0.24
G3P	Ctrl	7.465 ± 5.031	1.78 ± 0.01	133.04 ± 89.43	0 ± 0	133.04 ± 89.43
	Stim	2.962 ± 0.954	0.73 ± 0	38.23 ± 15.29	−150.08 ± 197.24	188.32 ± 212.33
G3P_21	Ctrl	109.956 ± 7.694	1.46 ± 0.14	1613.36 ± 266.88	0 ± 0	1613.36 ± 266.88
	Stim	46.649 ± 50.203	1.38 ± 0.25	1122.95 ± 605.54	−2110.24 ± 1439.57	3233.19 ± 862.22
G3P_22	Ctrl	38.481 ± 43.378	7.61 ± 0.18	2887.22 ± 3202.21	0 ± 0	2887.22 ± 3202.21
	Stim	15.014 ± 3.308	6.68 ± 0.63	1855.18 ± 1626.69	−782.25 ± 1484.08	2637.43 ± 3108.14
HBA	Ctrl	17.237 ± 0.806	7.22 ± 0.11	1243.23 ± 46.1	0 ± 0	1243.23 ± 46.1
	Stim	47.533 ± 4.778	8.14 ± 0.22	2639.76 ± 282.65	1009.87 ± 147.66	1629.89 ± 150.76
HBB1	Ctrl	2.128 ± 1.269	5.6 ± 0.26	118.19 ± 70.19	0 ± 0	118.19 ± 70.19
	Stim	4.543 ± 1.111	6.75 ± 0.22	225.26 ± 17.63	80.5 ± 78.44	144.75 ± 81.5
HBB2	Ctrl	1.274 ± 1.127	6.86 ± 0.5	85.82 ± 77.22	0 ± 0	85.82 ± 77.22
	Stim	1.235 ± 0.526	6.08 ± 1.46	76.4 ± 29.18	−1.3 ± 51.95	77.7 ± 67.98
HINT1	Ctrl	4.597 ± 0.916	1.53 ± 0.24	70.73 ± 19.3	0 ± 0	70.73 ± 19.3
	Stim	4.486 ± 0.713	1.41 ± 0.26	63.79 ± 10.13	−3.68 ± 46.57	67.47 ± 56.58
HSPB6	Ctrl	11.222 ± 1.729	2.49 ± 0.27	276.83 ± 13.17	0 ± 0	276.83 ± 13.17
	Stim	19.072 ± 2.131	4.31 ± 0.31	649.46 ± 38.23	261.67 ± 28.4	387.79 ± 26.73
IDH3A	Ctrl	11.921 ± 3.248	3.16 ± 0.16	380.38 ± 122.29	0 ± 0	380.38 ± 122.29
	Stim	10.4 ± 0.726	3.87 ± 0.13	430.66 ± 38.97	−50.71 ± 126.53	481.37 ± 164.29
IDHP	Ctrl	51.897 ± 4.565	5.24 ± 0.22	2725.77 ± 350.74	0 ± 0	2725.77 ± 350.74
	Stim	50.702 ± 0.872	5.39 ± 0.3	2771.17 ± 299.85	−39.84 ± 125.14	2811 ± 424.06
KAD1	Ctrl	28.059 ± 4.147	1.76 ± 0.02	493.58 ± 74.94	0 ± 0	493.58 ± 74.94
	Stim	29.437 ± 3.087	1.56 ± 0.12	445.81 ± 23.08	45.93 ± 165.84	399.88 ± 188.47
KCRB	Ctrl	30.595 ± 10.302	5.75 ± 0.6	1791.07 ± 713.95	0 ± 0	1791.07 ± 713.95
	Stim	10.018 ± 4.301	4.69 ± 0.43	969.71 ± 379.84	−685.9 ± 296.54	1655.61 ± 619.91
KCRM	Ctrl	96.04 ± 13.516	4.67 ± 0.18	4494.59 ± 794.43	0 ± 0	4494.59 ± 794.43
	Stim	87.555 ± 9.66	4.67 ± 0.11	4293.57 ± 634.8	−282.82 ± 152.48	4576.39 ± 763.69
KCRM_16	Ctrl	413.051 ± 36.2	5.27 ± 0.15	21782.28 ± 2488.87	0 ± 0	21782.28 ± 2488.87
	Stim	198.73 ± 44.331	5.21 ± 0	15946.53 ± 2086.16	−7144.05 ± 287.86	23090.57 ± 1817.23
KCRM_17	Ctrl	423.389 ± 40.41	3.44 ± 0.22	14632.6 ± 2318.62	0 ± 0	14632.6 ± 2318.62
	Stim	192.577 ± 22.55	3.57 ± 0.04	10977.08 ± 993.4	−7693.73 ± 615.67	18670.81 ± 1593.69
KCRS_18	Ctrl	450.377 ± 30.738	3.62 ± 0.08	16319.94 ± 1091.25	0 ± 0	16319.94 ± 1091.25
	Stim	210.019 ± 58.468	4.81 ± 0.24	15911.32 ± 2667.71	−8011.93 ± 1242.93	23923.25 ± 1619.45
KCRS_19	Ctrl	431.301 ± 41.392	2.12 ± 0.02	9156.49 ± 802.23	0 ± 0	9156.49 ± 802.23
	Stim	302.168 ± 42.54	4.51 ± 0.28	16547.62 ± 1006.77	−4304.43 ± 2789.78	20852.05 ± 1842.02

(Continues)

TABLE 2 (Continued)

Identifier	Group	ABD (μg)	FSR (%/d)	ASR (ng/d)	ABR (ng/d)	ADR (ng/d)
KPYM	Ctrl	79.697 ± 10.195	2.36 ± 0.33	1892.16 ± 454.83	0 ± 0	1892.16 ± 454.83
	Stim	87.21 ± 9.936	2.15 ± 0.1	1796.88 ± 278.44	250.44 ± 207.76	1546.43 ± 319.5
LDHA	Ctrl	108.089 ± 6.786	11.53 ± 0.05	12457.11 ± 725.6	0 ± 0	12457.11 ± 725.6
	Stim	108.93 ± 7.088	11.28 ± 0.05	12241.4 ± 731.2	28.03 ± 15.47	12213.37 ± 721.1
MDHC	Ctrl	35.322 ± 1.773	3.67 ± 0.29	1295.17 ± 83.16	0 ± 0	1295.17 ± 83.16
	Stim	59.694 ± 6.675	4.74 ± 0.15	2257.03 ± 242.6	812.4 ± 219.43	1444.64 ± 127.46
MDHM	Ctrl	104.639 ± 10.927	10.37 ± 0.36	10864.93 ± 1420.18	0 ± 0	10864.93 ± 1420.18
	Stim	101.162 ± 16.945	10.74 ± 0.19	11069.56 ± 1608.18	−115.92 ± 345.51	11185.47 ± 1407.81
MLRS_11	Ctrl	643.988 ± 47.953	2.79 ± 0.13	17917.39 ± 992.05	0 ± 0	17917.39 ± 992.05
	Stim	48.939 ± 9.327	2.73 ± 0	9467.28 ± 770.76	−19834.97 ± 1295.96	29302.25 ± 2065.49
MLRS_12	Ctrl	1092.033 ± 88.234	1.63 ± 0.03	17845.66 ± 1726.12	0 ± 0	17845.66 ± 1726.12
	Stim	546.79 ± 648.837	1.81 ± 0.12	14661.57 ± 4665.12	−18174.75 ± 22945.56	32836.33 ± 18692.55
MYG	Ctrl	68.438 ± 4.668	2.31 ± 0.01	1582.6 ± 102.28	0 ± 0	1582.6 ± 102.28
	Stim	92.796 ± 7.03	3.64 ± 0.14	2936.55 ± 322.12	811.93 ± 79.05	2124.62 ± 243.09
MYL1	Ctrl	3.3 ± 1.605	1.87 ± 0.09	62.21 ± 30.83	0 ± 0	62.21 ± 30.83
	Stim	1.027 ± 0.041	1.64 ± 0.11	35.66 ± 14.22	−75.78 ± 52.15	111.45 ± 66.29
MYL1_10	Ctrl	538.363 ± 47.761	3.35 ± 0.31	18094.78 ± 3198.32	0 ± 0	18094.78 ± 3198.32
	Stim	254.257 ± 49.148	3.34 ± 0	13224.96 ± 1413.62	−9470.19 ± 1587.13	22695.16 ± 2082.41
MYL1_8	Ctrl	433.414 ± 83.669	4.8 ± 0.01	20795.97 ± 3986.39	0 ± 0	20795.97 ± 3986.39
	Stim	180.728 ± 100.254	4.55 ± 0.12	13953.58 ± 3498.09	−8422.84 ± 3334.77	22376.42 ± 4562.5
MYL1_9	Ctrl	569.734 ± 47.311	3.32 ± 0.05	18912.88 ± 1859	0 ± 0	18912.88 ± 1859
	Stim	278.664 ± 64.528	3.21 ± 0.18	13567.32 ± 802.91	−9702.35 ± 2890.2	23269.67 ± 3278.51
ODPA	Ctrl	23.355 ± 2.406	7.84 ± 0.27	1829.51 ± 191.95	0 ± 0	1829.51 ± 191.95
	Stim	37.202 ± 8.219	8.71 ± 0.58	2651.43 ± 524.2	461.58 ± 297.93	2189.85 ± 289.56
PARK7	Ctrl	10.306 ± 1.133	1.33 ± 0.04	137.31 ± 15.06	0 ± 0	137.31 ± 15.06
	Stim	10.538 ± 1.672	1.35 ± 0.21	139.58 ± 19.64	7.71 ± 49	131.86 ± 63.94
PFKAM	Ctrl	23.761 ± 3.78	9.25 ± 1.23	2219.7 ± 570.49	0 ± 0	2219.7 ± 570.49
	Stim	1.113 ± 0.354	8.15 ± 1.07	1023.69 ± 251.27	−754.96 ± 134.27	1778.64 ± 374.95
PGAM2	Ctrl	76.615 ± 4.639	5.38 ± 0.36	4131.95 ± 527.36	0 ± 0	4131.95 ± 527.36
	Stim	79.621 ± 15.464	5.17 ± 0.4	4069.18 ± 828.78	100.22 ± 366.07	3968.97 ± 473.77
PGK1	Ctrl	101.157 ± 5.766	6.53 ± 0.33	6588.74 ± 39.8	0 ± 0	6588.74 ± 39.8
	Stim	116.618 ± 15.583	5.6 ± 0.34	6117.53 ± 973.99	515.38 ± 330.12	5602.16 ± 649.8
PGM1	Ctrl	35.586 ± 6.006	3.5 ± 0.2	1254.24 ± 281.39	0 ± 0	1254.24 ± 281.39
	Stim	55.338 ± 7.558	2.33 ± 0.22	1060.55 ± 86.56	658.77 ± 446.46	402.17 ± 524.73
PLEC_2	Ctrl	992.955 ± 85.984	0.56 ± 0.12	5583.69 ± 1705.98	0 ± 0	5583.69 ± 1705.98
	Stim	452.594 ± 93.357	0.94 ± 0.05	6795.43 ± 947.86	−18012.03 ± 333.63	24807.46 ± 856.1
PRVA	Ctrl	4.654 ± 0.666	4.5 ± 0.3	209.47 ± 35.09	0 ± 0	209.47 ± 35.09
	Stim	4.313 ± 0.872	4.09 ± 0.29	183.53 ± 16	−11.38 ± 51.08	194.91 ± 49.66
PYGB	Ctrl	57.895 ± 5.111	11.72 ± 0.97	6786.96 ± 793.09	0 ± 0	6786.96 ± 793.09
	Stim	22.199 ± 6.615	9.32 ± 1.49	3763.21 ± 899.76	−1189.85 ± 291.2	4953.07 ± 755.75
PYGM	Ctrl	186.593 ± 22.567	9.39 ± 0.41	17552.12 ± 2630.16	0 ± 0	17552.12 ± 2630.16
	Stim	189.128 ± 19.35	9.26 ± 0.39	17430.1 ± 2460.82	84.65 ± 483.34	17345.61 ± 2523.06
SAFB1	Ctrl	91.894 ± 5.005	0.98 ± 0	902.23 ± 50.35	0 ± 0	902.23 ± 50.35
	Stim	76.542 ± 20.555	1.24 ± 0.21	1027.89 ± 91.89	−511.73 ± 576.74	1539.62 ± 603.2

(Continues)

TABLE 2 (Continued)

Identifier	Group	ABD (μg)	FSR (%/d)	ASR (ng/d)	ABR (ng/d)	ADR (ng/d)
TNNI1_24	Ctrl	487.755 ± 40.23	3.35 ± 0.04	16344.8 ± 1555.22	0 ± 0	16344.8 ± 1555.22
	Stim	457.121 ± 169.884	3.86 ± 0.36	18019.22 ± 2339.75	−1021.14 ± 4322.32	19040.36 ± 2042.32
TNNI2_23	Ctrl	609.748 ± 50.768	4.29 ± 0.01	26179.54 ± 2109.51	0 ± 0	26179.54 ± 2109.51
	Stim	133.773 ± 45.309	2.22 ± 0.53	8156.02 ± 1254.36	−15865.83 ± 2206.8	24021.85 ± 1558.17
TNNT1_27	Ctrl	982.272 ± 82.957	1.36 ± 0.42	13591.82 ± 5319.01	0 ± 0	13591.82 ± 5319.01
	Stim	554.652 ± 326.11	2.19 ± 0.15	16976.49 ± 4704.14	−14254 ± 10451.25	31230.49 ± 7296.49
TNNT3_25	Ctrl	779.237 ± 65.412	2.66 ± 0.06	20716.24 ± 1262.76	0 ± 0	20716.24 ± 1262.76
	Stim	301.783 ± 162.126	2.47 ± 0.03	13321.96 ± 2567.46	−15915.15 ± 3679.44	29237.11 ± 1737.41
TNNT3_26	Ctrl	606.31 ± 88.137	1.83 ± 0.1	11114.15 ± 1631.94	0 ± 0	11114.15 ± 1631.94
	Stim	187.44 ± 12.098	0.75 ± 0	2958.49 ± 323.68	−13962.33 ± 3045.91	16920.83 ± 3358.22
TNNT3_28	Ctrl	644.558 ± 53.776	1.64 ± 0.15	10642.15 ± 1880.09	0 ± 0	10642.15 ± 1880.09
	Stim	148.006 ± 11.68	1.18 ± 0.46	4764.17 ± 2186.4	−16551.73 ± 1668.5	21315.9 ± 3854.9
TPIS	Ctrl	58.074 ± 3.245	2.05 ± 0.04	1187.22 ± 42.24	0 ± 0	1187.22 ± 42.24
	Stim	12.737 ± 2.265	0.93 ± 0.02	327.55 ± 18.18	−1511.24 ± 65.93	1838.79 ± 75.84
TPM2_7	Ctrl	3363.008 ± 293.726	1.31 ± 0.08	44066.39 ± 6466.91	0 ± 0	44066.39 ± 6466.91
	Stim	1539.928 ± 278.791	1.39 ± 0.08	34157.75 ± 4805.09	−60769.34 ± 3955.03	94927.09 ± 5386.44
TPM4_6	Ctrl	3146.903 ± 311.36	9.32 ± 0.29	292795.95 ± 20066.72	0 ± 0	292795.95 ± 20066.72
	Stim	1521.797 ± 136.055	9.1 ± 0.1	212405.22 ± 19859.46	−54170.21 ± 5924.03	266575.42 ± 25624.58
VDAC	Ctrl	31.607 ± 1.529	1.56 ± 0.02	493.74 ± 27.07	0 ± 0	493.74 ± 27.07
	Stim	32.247 ± 4.065	1.52 ± 0.26	482.47 ± 49.62	21.33 ± 134.62	461.14 ± 169.18

Note: Identifier represents the UniProt identifier and 2DGE spot number of each proteoform, Total abundance (ABD) is presented (μg). Fractional synthesis rate (FSR, %/d) was calculated across 0, 10, 20 and 30 days using Equation (3). Absolute rate of abundance change (ABR), synthesis (ASR) and degradation (ADR) are presented in ng/d.

CLFS was associated with proteoform-specific changes to the fast-twitch isoform of skeletal muscle myosin regulatory light chain (MLRS). Two proteoforms MLRS_11 and MLRS_12 were identified by 2DGE (Figure S1). The abundance of MLRS_12 was not altered by CLFS whereas MLRS_11 abundance decreased at a rate of 19.84 μg/ d from 644 μg in Ctrl to 49 μg in Stim during the course of the 30-day experiment. The difference in MLRS_11 ASR between Stim (9.47 μg/d) and Ctrl (17.92 μg/d) was 8.45 μg/d. Whereas the difference in MLRS_11 ADR between Stim (29.30 μg/d) and Ctrl (17.92 μg/d) was 11.39 μg/d (Figure 2F). Therefore, the 8.45 μg/d lesser ASR combined with the 11.39 μg/d increase in ADR accounts for the 19.385 μg/d change in MLRS_11 abundance. In percentage terms, the contribution of the change in synthesis to the change in abundance was 42.6% and the contribution of degradation to the change in abundance was 57.4%. Site-specific posttranslational modifications of MLRS were investigated by LC-MS/MS analysis of MLRS_11 and MLRS_12. A sequence coverage of 92% (MOWSE score 1770) was achieved and searches of the MS/MS spectra (Supporting Information) unambiguously identified S^{16} phosphorylation in both MLRS_11 and MLRS_12. In addition, MLRS_11 contained an additional site-specific phosphorylation of S^{20} (Figure S2) and a di-glycine remnant on K^{137} (Figure S3) that were not detected in MLRS_12.

The relative contribution of synthesis and degradation to changes in protein abundance differed on a protein-by-protein basis and between each 10-d interval within the 30-d experimental period. Figure 3 illustrates the relative contributions of synthesis and degradation to changes in protein abundance between day 0 and day 10 (Figure 3A,B), day 10 and day 20 (Figure 3C,D), or between day 20 and day 30 (Figure 3E,F). On average protein degradation accounted for 64.34% of the change in protein abundance between day 0 and day 10, whereas the contribution of degradation was 54.52% between day 10 and day 20, and the contribution of degradation was 53.47% between day 20 and day 30 of CLFS. The contribution of degradation to changes in the abundance of individual proteins was different during each 10-d period of the experiment. The majority of the change in MLRS_11 abundance was complete after 20 days CLFS. The abundance (41.31 ± 36.37 μg) of MLRS_11 was significantly ($P = .00106$) less than control (235.05 ± 15.38 μg) after 20 days of CLFS. During the period between 10 and 20 days (Figure 3C,D) the difference in degradation between Ctrl and Stim EDL accounted for 92.7% of the change in MLRS_11 abundance.

4 | DISCUSSION

We report novel data on the absolute rates (ng/d) of protein synthesis, abundance-change and degradation in muscle undergoing adaptation to a chronic exercise stimulus in vivo. Proteo-ADPT offers new insight to the processes that result in changes in protein abundance and, therefore, muscle function induced by chronic endurance activity. Alterations to the abundance of key myofibrillar and metabolic enzymes in exercised muscle were underpinned by significant changes

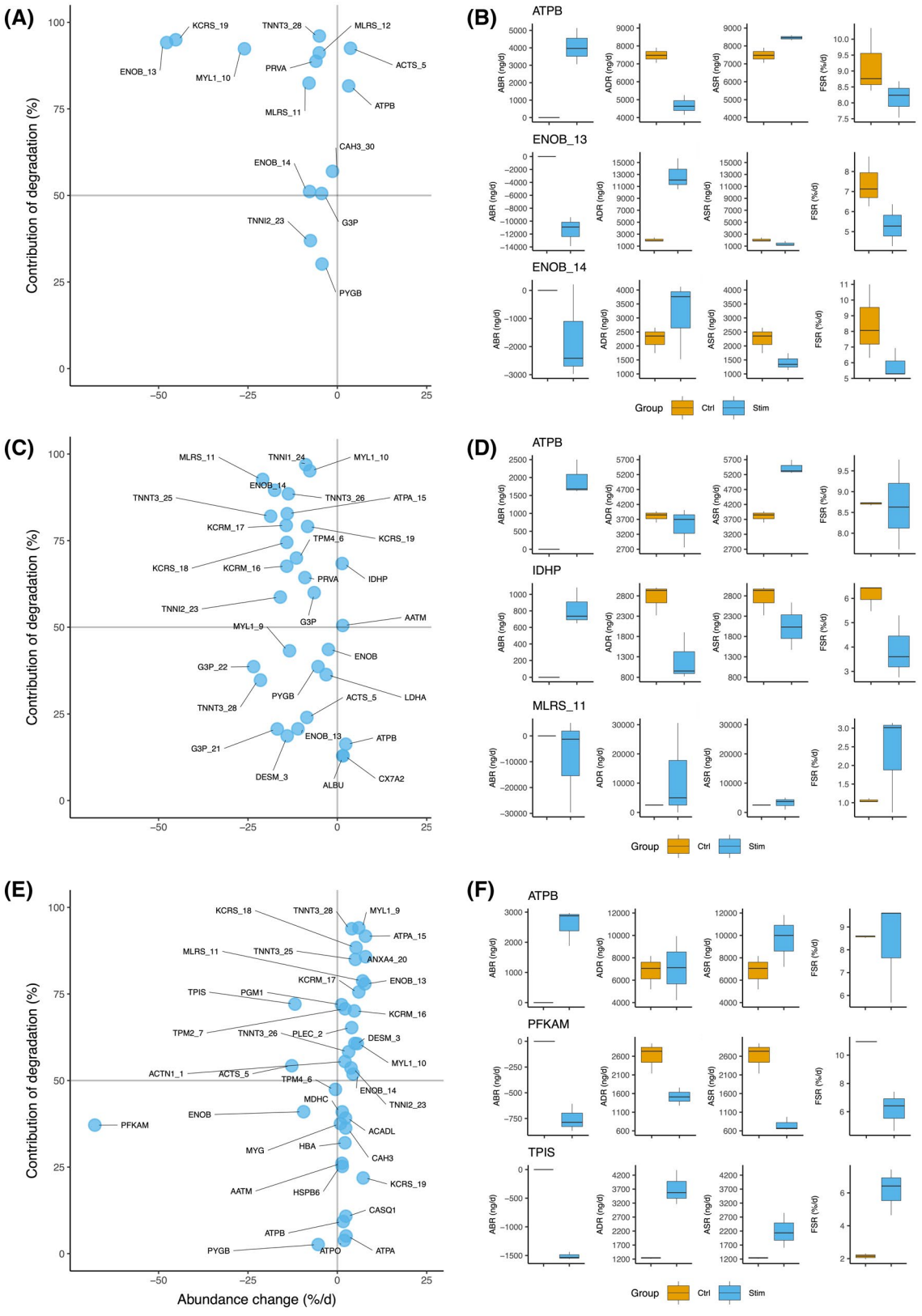

FIGURE 3 Temporal differences in the contribution of protein degradation to changes in the abundance of individual proteins. Scatter plots reporting the percent contribution of degradation to changes in protein abundance presented as the rate (ng/d) of change in abundance expressed as a percentage of average protein abundance during (A) 0 and 10 days, (C) 10 and 20 days or (E) 20 and 30 days periods of CLFS. Box plots reporting the rates (ng/d) of change in abundance (ABR), absolute synthesis rate (ASR), absolute degradation rate (ADR) and FSR (%/d) for select proteins (ATPB, ATP synthase subunit beta; ENOB, beta enolase; IDHP, isocitrate dehydrogenase; MLRS, myosin regulatory light chain 2; PFKAM, ATP-dependant 6-phosphofructokinase; TPIS, triosephosphate isomerase) during (B) 0 and 10 days, (D) 10 and 20 days or (F) 20 and 30 days periods of CLFS. Proteins are labeled by their UniProt identifier in panels A, C and E. Panel A reports proteins that differed in abundance at a significance level of $P < .1$, whereas panels C and E report proteins that changed in abundance at a significance level of $P < .05$ after BH-correction

to the rates of both synthesis and degradation (Figure 2). Moreover, the relative contributions of synthesis and degradation to protein-by-protein changes in abundance were different during early, mid and late periods of the experimental intervention (Figure 3). In response to CLFS, fast-twitch EDL muscle transformed to a slower more oxidative phenotype through decreases in the abundance of glycolytic enzymes and fast isoforms of myofibrillar proteins and cooccurring increases in mitochondrial proteins and slow myofibrillar protein-isoforms. The contribution of protein degradation to changes in muscle protein abundance averaged 49% and some changes in protein abundance were almost entirely due to a change in protein degradation, rather than a change in protein synthesis. The ability to identify which changes in protein abundance are primarily mediated by either synthetic or degradative processes provides new opportunities for future work linking regulatory mechanisms, such as ubiquitination, with signal transduction processes and the expression of ubiquitin E3 ligases.

Muscle adaptations to endurance training occur gradually and involve the activation of signaling networks and gene expression programes that result in long-term changes in muscle phenotype. The outcomes of endurance training, including changes to muscle substrate utilization and mitochondrial content are well established[26] but the acute and chronic responses of the muscle proteome to exercise differ[27,28] and cannot easily be reconciled. Early signaling responses to acute exercise[29] and the subsequent changes in gene expression[20] have been investigated in detail. Whereas, the intervening processes that join acute responses of each individual bout of exercise into cumulative adaptation have not received so much attention. In humans, changes in the abundance of proteins and mRNA after a chronic period of training correlate poorly[20] and mRNA responses to acute exercise do not predict longer term adaptations of the muscle proteome.[30] These findings resonate with acknowledged discrepancies between the abundance of proteins and the expression of their mRNA in model organisms.[31] Data from mammalian cells in vitro[32] report the generally poor correlation between mRNA and protein can only be resolved when both protein synthesis and degradation rates are taken in to account. Proteo-ADPT enables the synthesis-abundance-degradation relationship of proteins to be studied so that the contribution of protein degradation can be assessed in vivo and may be key in linking cell signaling events to protein degradative processes. The ubiquitin proteasome system is established as a regulatory mechanism influencing the abundance of short-lived proteins, including the myogenic transcription factor, Myo D 1.[33] Substrates of key ubiquitin E3 ligases in muscle, including atrogin-1[34] and MuRF1,[35] have been reported, but there are >1,400 E3 ubiquitin-protein ligases and >800 autophagy-related proteins annotated in the Human SwissProt database. The ubiquitin proteasome[36] and autophagy[37] systems are established components in the adaptation of muscle to exercise, and acute exercise causes widespread changes in protein ubiquitination.[38] The contribution of protein-specific degradation to exercise-induced changes in the profile of abundant muscle proteins has seldom been reported but this information will be essential to further understanding of the health benefits of exercise.

Recently, we[5,39] developed dynamic proteome profiling (DPP) and investigated protein-specific responses of human muscle to resistance training[10] and rat muscle to endurance activity.[40] In the current work, we have calculated absolute (ng) values and used time series analysis[41] to exclude proteins that fitted poorly ($R^2 < 0.85$) to the expected exponential decay in peptide monoisotopic peak abundance. These methodological developments have enabled us to interrogate each 10-d interval with confidence and reveal time-dependent differences in the contributions of synthesis and degradation to add further detail to exercise-induced changes in protein abundance and synthesis rate. We report a 2.69-fold increase ($P = .0044$ BH-corrected) in ATPA abundance (Figure 1F) and a 120% increase in the FSR of ATPA from 1.44 ± 0.23 to 3.16 ± 0.03%/d in EDL exposed to 30-d CLFS (Figure 2). These data derived from our extreme model of change give insight to how adaptation of ATPA might be orchestrated in the context of endurance exercise. For example, our recent analysis of voluntary free-wheel running [40] reported a 28% increase in the FSR of ATPA from 1.86 ± 0.07%/d to 2.38 ± 1.3%/d in rat slow-twitch muscle. Free-wheel running is a mild training stimulus and did not alter ATPA protein abundance[40] but increases in the abundance of ATP synthase subunits are a common finding in proteomic studies of moderate to intense endurance training.[27] However, based on FSR data alone, it is not possible to interpret how the increase in

ATPA synthesis contributed to the gain in ATPA abundance. Nor is it clear whether a change in ATPA degradation rate may have contributed to or detracted from the synthetic response. In the current study, we equate FSR measurements with absolute protein abundance data and report the 7.6 ± 0.3 μg/d gain in ATPA abundance was almost entirely accounted for by the greater ($P = .0072$ BH-corrected) synthesis of ATPA in Stim (6.3 ± 0.9 μg/d) than Ctrl (1.2 ± 0.2 μg/d) muscle, and a decline in protein degradation contributed to rather than detracted from this response.

Our DPP study[10] on human muscle responses to resistance exercise highlighted several different patterns among the synthesis, abundance, and degradation responses of individual proteins. For example, glyceraldehyde-3-phosphate dehydrogenase (G3P) and triosephosphate isomerase (TPIS) decreased in abundance without exhibiting a decrease in FSR, whereas the significant decrease in beta-enolase (ENOB) abundance in resistance-trained muscle occurred alongside a significant increase in ENOB synthesis rate.[10] These findings warranted further investigation on the role and regulation of protein degradation in exercise-induced muscle adaptation. Using Proteo-ADPT, we report instances where the difference in protein degradation almost entirely accounted for the change in protein abundance. For example, during the first 10 days of CLFS the lesser degradation of ATPB was responsible for 82% of the gain in ATPB abundance. The turnover (7.9 ± 0.98 μg/d) of ATPB was stable in Ctrl muscle, whereas ATPB synthesis increased to 8.74 ± 0.5 μg/d in Stim muscle and degradation decreased to 4.62 ± 0.55 μg/d resulting in a gain ($P = .012$) in ATPB abundance from 87.3 ± 6.8 μg to 127.9 ± 14.6 μg. Notably, the FSR of ATPB was greater in Ctrl (9.16 ± 1.04%/d) than Stim (8.15 ± 0.57%/d) muscle (Figure 3D). Indeed, 20% of proteins studied exhibited opposite changes in FSR and ASR in Stim muscle during the course of the 30-d intervention (Table 2). These observations serve to highlight the challenges of interpreting protein-specific FSR data in isolation, and the added benefits of calculating absolute data on the total abundance change, synthesis rate and degradation rate of individual proteins.

Muscle responses to endurance exercise in rats[2] and humans[3] include changes to the proteoform abundance of myofibrillar and metabolic proteins that may indicate differences in the expression or posttranscriptional processing of splice variants or changes to the posttranslational state of proteins.[21] Our current 2DGE analysis of myofibrillar proteins discovered proteoform-specific differences in the basal rate of turnover among proteoforms in Ctrl muscle, and differences in the contributions of synthesis and degradation to changes in proteoform abundance in Stim muscle. We report a di-glycine remnant on K^{137} and phosphorylation of S^{20} of myosin regulatory light chain (MLRS) are associated with the reduction in MLRS_11 abundance that was primarily driven by a greater rate of degradation in Stim muscle. Ubiquitination of MLRS K^{137} has previously been reported[42] in mouse muscle undergoing denervation-induced atrophy and was not detected in innervated control samples. Cross-talk exists between phosphorylation and ubiquitination in exercised muscle[38] and phosphorylation of MLRS has previously been associated with age-related decline in muscle function.[43] Therefore, our findings point to a potential link between S^{20} phosphorylation and ubiquitination of K^{137} that warrants further investigation. Bottom-up analysis of peptides enriched using anti-diglycine remnant (K-ε-GG) Ab[44] and titanium dioxide[22] could provide more comprehensive insight to site-specific changes in ubiquitination and phosphorylation, respectively. Nevertheless, top-down analyses will also be required to capture the unique combinations of covalent modifications that cooccur among different regions of each protein. In addition, it will be important to characterize the topology[23] and posttranslational modification[45] of polyubiquitin chains anchored to specific protein residues to fully understand the biological consequences of the protein modifications.

Thirty days CLFS reduced the size of Stim EDL to 50% of Ctrl (Figure 1A). Previously, we[13] reported a similar loss in EDL mass after 56 days of CLFS was associated significant changes to the myofiber profile and functional characteristics of rat EDL. Maximum isometric force decreased to 40% of control and time to peak isometric tension increased by 54%, resulting in a ~ 74% decrease in maximum power of transformed EDL. After 56 days of CLFS, the changes in muscle function coincided with a significant increase in the proportion of Type I fibers and decreases in the proportion and cross-sectional area of Type IIB fibers in stimulated muscle.[13] There was no evidence of muscle damage after 9 or 56 days CLFS[13] and in our current work we report decreases in the absolute abundance of metabolic enzymes and slow- as well as fast- myofibrillar isoforms that account for up to 90% of the decline in muscle protein content. Our current analysis was limited to highly abundant proteins but nevertheless did not include collagens, which are an important component of the skeletal muscle extracellular matrix.[46] Onward development of Proteo-ADPT using more advanced mass spectrometry platforms may need to consider sample preparation methods suitable for muscle collagens. Alternatively, fractionation may be required to distinguish the cell-specific origin of newly synthesized collagen peptides.

Pette et al[47] also reported reciprocal changes in MyHC IIb and MyHC IIa in Stim rat EDL. After 30 days CLFS. The relative abundance of MyHC IIa increased from ~18% to 46% and MyHC IIb abundance decreased from ~47% to ~16%, whereas the increase in MyHC I from ~5% to ~8% was less prominent.[47] Herein, we report the emergence of slow isoforms of myosin light chains and troponin subunits (Table 1) consistent with earlier histochemical[13] and biochemical[47] findings. Our current analysis also adds significant detail

to the mechanisms underpinning the previously observed changes in myofiber profile. For example, between 10 and 20 days CLFS the greater degradation of a proteoform of the slow skeletal isoform of troponin I (TNNI1_24) accounted for 97% of the decrease in TNNI1_24 abundance in Stim EDL. Whereas a decrease in synthetic rate accounted for 65% of the decrease in the abundance of the fast isoform of troponin T (TNNT3_28), which likely reflects expected decreases in fast troponin T gene expression.[48] Mayne et al[49], reports the appearance of slow twitch myosin light chain isoforms in rat EDL after 61 days CLFS. Herein, we reveal emergent slow isoforms of myofibrillar proteins (Table 1) were not spared from degradation and their rate of synthesis exceeded the rate of gain in abundance. This pattern of response agrees closely with the observation[50] that the increase in relative abundance of MyHC IIa during the first 15 days of CLFS lags behind the rate of increase in the incorporation of ^{35}S-methionine in to the IIa MyHC pool. Our protein abundance data also concur with proteomic profiling[51] of rabbit fast-twitch muscle responses to CLFS that report a transition from fast to slow isoforms of myofibrillar proteins alongside decreases in glycolytic enzymes and increases in mitochondrial proteins. Moreover, the emergence of CRYAB and MLRV in Stim EDL (Table 1) is consistent with our findings in the fast-twitch plantaris muscle of endurance-trained rats.[2] The emergence of CRYAB among the myofibrillar fraction is similar to the response in resistance trained human muscle[10] and may be associated with a protective effect evoked by muscle contraction.[52]

In conclusion, we provide empirical data on the contribution of protein degradation and protein synthesis to physiological adaptation of skeletal muscle. Over the course of the 30 days CLFS intervention, protein degradation made a 49% contribution to the changes in muscle protein abundance. Generally, proteins that decreased in abundance had a greater contribution of degradation to the change in abundance. However, some proteins decrease in abundance with very little change in degradation rate, that is, the decrease in protein synthesis almost fully explained the decrease in abundance. Conversely, the increased abundance of some proteins was primarily due to a lesser rate of degradation rather than a greater rate of synthesis. Muscle adaptations to endurance exercise underpin many of the health benefits of a physically active lifestyle. Nevertheless, the processes governing changes in protein abundance are incompletely understood. Proteo-ADPT provides unique insight to the contributions of synthetic and degradative processes to exercise-induced changes in protein abundance. This information can be used to link signaling events to the control of either synthetic or degradative effects and to resolve disparities between studies that measure gene expression and studies that measure changes in protein abundance in response to exercise.

CONFLICT OF INTEREST

The authors declare no conflicts of interest.

AUTHOR CONTRIBUTIONS

JG Burniston, JC Jarvis, and PJ Lisboa designed the research. SJ Hesketh, H. Sutherland, JC Jarvis, and JG Burniston performed the research. SJ Hesketh, PJ Lisboa, and JG Burniston analyzed the data. SJ Hesketh, JC Jarvis, and JG Burniston wrote the paper.

ORCID

Jatin G. Burniston https://orcid.org/0000-0001-7303-9318

REFERENCES

1. Holloszy JO. Biochemical adaptations in muscle. Effects of exercise on mitochondrial oxygen uptake and respiratory enzyme activity in skeletal muscle. *J Biol Chem*. 1967;242:2278-2282.
2. Burniston JG. Changes in the rat skeletal muscle proteome induced by moderate-intensity endurance exercise. *Biochim Biophys Acta—Proteins Proteomics*. 2008;1784:1077-1086.
3. Holloway KV, Gorman MO, Woods P, et al. Proteomic investigation of changes in human vastus lateralis muscle in response to interval-exercise training. *Proteomics*. 2009;9:5155-5174.
4. Nilsson A, Björnson E, Flockhart M, Larsen FJ, Nielsen J. Complex I is bypassed during high intensity exercise. *Nat Commun*. 2019;10:5072.
5. Burniston JG. Investigating muscle protein turnover on a protein-by-protein basis using dynamic proteome profiling. In: Burniston JG, Chen Y, eds. *Omics approaches to understanding muscle biology*. New York, NY: Springer; 2019:171-190.
6. Wilkinson SB, Phillips SM, Atherton PJ, et al. Differential effects of resistance and endurance exercise in the fed state on signalling molecule phosphorylation and protein synthesis in human muscle. *J. Physiol*. 2008;586:3701-3717.
7. Phillips SM, Tipton KD, Aarsland A, et al. Mixed muscle protein synthesis and breakdown after resistance exercise in humans. *Am J Physiol-Endocrinol Metab*. 1997;273(1):E99-107.
8. Short KR, Vittone JL, Bigelow ML, Proctor DN, Nair KS. Age and aerobic exercise training effects on whole body and muscle protein metabolism. *Am J Physiol Endocrinol Metab*. 2004;286:E92-101.
9. Shankaran M, King CL, Angel TE, et al. Circulating protein synthesis rates reveal skeletal muscle proteome dynamics. *J Clin Invest*. 2016;126:288-302.
10. Camera DM, Burniston JG, Pogson MA, Smiles WJ, Hawley JA. Dynamic proteome profiling of individual proteins in human skeletal muscle after a high-fat diet and resistance exercise. *FASEB J*. 2017;31:5478-5494.
11. Kosek DJ. Efficacy of 3 days/wk resistance training on myofiber hypertrophy and myogenic mechanisms in young vs. older adults. *J Appl Physiol*. 2006;101:531-544.
12. Pette D, Vrbová G. The contribution of neuromuscular stimulation in elucidating muscle plasticity revisited. *Eur J Transl Myol*. 2017;27:33-39.
13. Jarvis JC, Mokrusch T, Kwende MMN, Sutherland H, Salmons S. Fast-to-slow transformation in stimulated rat muscle. *Muscle Nerve*. 1996;19:1469-1475.

14. Busch R, Kim Y-K, Neese RA, et al. Measurement of protein turnover rates by heavy water labeling of nonessential amino acids. *Biochim Biophys Acta*. 2006;1760:730-744.
15. Li L, Nelson CJ, Solheim C, Whelan J, Millar AH. Determining degradation and synthesis rates of arabidopsis proteins using the kinetics of progressive 15 N labeling of two-dimensional gel-separated protein spots. *Mol Cell Proteomics*. 2012;11:1-16.
16. Silva JC, Gorenstein MV, Li G, Vissers JPC, Geromanos SJ. Absolute Quantification of Proteins by LCMS E. *Mol Cell Proteomics*. 2006;5:144-156.
17. Salmons S, Jarvis JC. Simple optical switch for implantable devices. *Med Biol Eng Comput*. 1991;29:554-556.
18. Hesketh S, Srisawat K, Sutherland H, Jarvis JC, Burniston JG. On the rate of synthesis of individual proteins within and between different striated muscles of the rat. *Proteomes*. 2016;4:12.
19. Wisniewski JR, Zougman A, Nagaraj N, Mann M, Wi JR. Universal sample preparation method for proteome analysis. *Nat Methods*. 2009;6:362-377.
20. Sollanek KJ, Burniston JG, Kavazis AN, et al. Global proteome changes in the rat diaphragm induced by endurance exercise training. *PLoS One*. 2017;12:1-21.
21. Bowden-Davies K, Connolly J, Burghardt P, Koch LG, Britton SL, Burniston JG. Label-free profiling of white adipose tissue of rats exhibiting high or low levels of intrinsic exercise capacity. *Proteomics*. 2015;15:2342-2349.
22. Burniston JG, Connolly J, Kainulainen H, Britton SL, Koch LG. Label-free profiling of skeletal muscle using high-definition mass spectrometry. *Proteomics*. 2014;14:2339-2344.
23. Malik Z, Cobley J, Morton J, et al. Label-free LCMS profiling of skeletal muscle reveals heart-type fatty acid binding protein as a candidate biomarker of aerobic capacity. *Proteomes*. 2013;1:290-308.
24. Holmes WE, Angel TE, Li KW, Hellerstein MK. Dynamic proteomics. In vivo proteome-wide measurement of protein kinetics using metabolic labeling. *Methods Enzymol*. 2015;561:219-276.
25. Gerner C, Vejda S, Gelbmann D, et al. Concomitant determination of absolute values of cellular protein amounts, synthesis rates, and turnover rates by quantitative proteome profiling. *Mol Cell Proteomics*. 2002;1:528-537.
26. Holloszy JO, Coyle EF. Adaptations of skeletal muscle to endurance exercise and their metabolic consequences. *J Appl Physiol*. 2016;121:831-838.
27. Burniston JG, Hoffman EP. Proteomic responses of skeletal and cardiac muscle to exercise. *Expert Rev Proteomics*. 2011;8:361-377.
28. Schild M, Ruhs A, Beiter T, et al. Basal and exercise induced label-free quantitative protein profiling of m. vastus lateralis in trained and untrained individuals. *J Proteomics*. 2015;122:119-132.
29. Hoffman NJ, Parker BL, Chaudhuri R, et al. Global phosphoproteomic analysis of human skeletal muscle reveals a network of exercise-regulated kinases and AMPK substrates. *Cell Metab*. 2015;22:922-935.
30. Makhnovskii PA, Zgoda VG, Bokov RO, et al. Regulation of proteins in human skeletal muscle: the role of transcription. *Sci Rep*. 2020;1-9.
31. Liu Y, Beyer A, Aebersold R. On the dependency of cellular protein levels on mRNA abundance. *Cell*. 2016;165:535-550.
32. Kristensen AR, Gsponer J, Foster LJ. Protein synthesis rate is the predominant regulator of protein expression during differentiation. *Mol Syst Biol*. 2013;9:1-12.
33. Abu Hatoum O, Gross-Mesilaty S, Breitschopf K, et al. Degradation of myogenic transcription factor MyoD by the ubiquitin pathway in vivo and in vitro: regulation by specific DNA binding. *Mol Cell Biol*. 1998;18:5670-5677.
34. Tintignac LA, Lagirand J, Batonnet S, Sirri V, Leibovitch MP, Leibovitch SA. Degradation of MyoD mediated by the SCF (MAFbx) ubiquitin ligase. *J Biol Chem*. 2005;280:2847-2856.
35. Cohen S, Brault JJ, Gygi SP, et al. During muscle atrophy, thick, but not thin, filament components are degraded by MuRF1-dependent ubiquitylation. *J Cell Biol*. 2009;185:1083-1095.
36. Cunha TF, Moreira JBN, Paixao NA, et al. Aerobic exercise training upregulates skeletal muscle calpain and ubiquitin-proteasome systems in healthy mice. *J Appl Physiol*. 2012;112:1839-1846.
37. He C, Bassik MC, Moresi V, et al. Exercise-induced BCL2-regulated autophagy is required for muscle glucose homeostasis. *Nature*. 2012;481:511-515.
38. Parker BL, Kiens B, Wojtaszewski JFP, Richter EA, James DE. Quantification of exercise-regulated ubiquitin signaling in human skeletal muscle identifies protein modification cross talk via NEDDylation. *FASEB J*. 2020;34(4):5906-5916. https://doi.org/10.1096/fj.202000075R
39. Srisawat K, Hesketh K, Cocks M, et al. Reliability of protein abundance and synthesis measurements in human skeletal muscle. *Proteomics*. 2019;20:1900194.
40. Holwerda AM, Bouwman FG, Nabben M, et al. Endurance-type exercise increases bulk and individual mitochondrial protein synthesis rates in rats. *Int J Sport Nutr Exerc Metab*. 2020;30:1-12.
41. Stead CA, Hesketh SJ, Bennett S, et al. Fractional synthesis rates of individual proteins in rat soleus and plantaris muscles. *Proteomes*. 2020;8:10.
42. Lang F, Aravamudhan S, Nolte H, et al. Dynamic changes in the mouse skeletal muscle proteome during denervation-induced atrophy. *Dis Model Mech*. 2017;10:881-896.
43. Wei L, Gregorich ZR, Lin Z, et al. Novel sarcopenia-related alterations in sarcomeric protein post-translational modifications (PTMs) in skeletal muscles identified by top-down proteomics. *Mol Cell Proteomics*. 2018;17:134-145.
44. Wagner SA, Beli P, Weinert BT, et al. A proteome-wide, quantitative survey of in vivo ubiquitylation sites reveals widespread regulatory roles. *Mol Cell. Proteomics*. 2011;10(M111):013284.
45. Okatsu K, Koyano F, Kimura M, et al. Phosphorylated ubiquitin chain is the genuine Parkin receptor. *J Cell Biol*. 2015;209:111-128.
46. Gillies AR, Lieber RL. Structure and function of the skeletal muscle extracellular matrix. *Muscle Nerve*. 2011;44:318-331.
47. Pette D, Sketelj J, Škorjanc D, Leisner E, Traub I, Bajrović F. Partial fast-to-slow conversion of regenerating rat fast-twitch muscle by chronic low-frequency stimulation. *J Muscle Res Cell Motil*. 2002;23:215-221.
48. Pette D. Effects of chronic electrostimulation on muscle gene expression. *Semin Thorac Cardiovasc Surg*. 1991;3:101-105.
49. Mayne CN, Mokrusch T, Jarvis JC, Gilroy SJ, Salmons S. Stimulation-induced expression of slow muscle myosin in a fast muscle of the rat. Evidence of an unrestricted adaptive capacity. *FEBS Lett*. 1993;327:297-300.
50. Termin A, Pette D. Changes in myosin heavy-chain isoform synthesis of chronically stimulated rat fast-twitch muscle. *Eur J Biochem*. 1992;204:569-573.
51. Donoghue P, Doran P, Wynne K, Pedersen K, Dunn MJ, Ohlendieck K. Proteomic profiling of chronic low-frequency stimulated fast muscle. *Proteomics*. 2007;7:3417-3430.

52. Paulsen G, Lauritzen F, Bayer ML, et al. Subcellular movement and expression of HSP27, αB-crystallin, and HSP70 after two bouts of eccentric exercise in humans. *J Appl Physiol*. 2009;107(2): 570-582.

SUPPORTING INFORMATION

Additional Supporting Information may be found online in the Supporting Information section.c

How to cite this article: Hesketh SJ, Sutherland H, Lisboa PJ, Jarvis JC, Burniston JG. Adaptation of rat fast-twitch muscle to endurance activity is underpinned by changes to protein degradation as well as protein synthesis. *The FASEB Journal*. 2020;00: 1–20. https://doi.org/10.1096/fj.202000668RR